THE UNIVERSITY OF ALBERTA

ULTIMATE STRENGTH OF COMPOSITE BEAMS IN NEGATIVE BENDING

by

© GREGORY VIRGINIO LEVER

A THESIS

SUBMITTED TO THE FACULTY OF GRADUATE STUDIES

IN PARTIAL FULFILMENT OF THE REQUIREMENTS FOR THE DEGREE OF

MASTER OF SCIENCE

DEPARTMENT OF CIVIL ENGINEERING

EDMONTON, ALBERTA
SPRING, 1970

UNIVERSITY OF ALBERTA

FACULTY OF GRADUATE STUDIES

The undersigned certify that they have read, and recommend to the Faculty of Graduate Studies for acceptance, a thesis entitled ULTIMATE STRENGTH OF COMPOSITE BEAMS IN NEGATIVE BENDING submitted by GREGORY VIRGINIO LEVER in partial fulfilment of the requirements for the degree of Master of Science.

ABSTRACT

The objectives of this investigation were to study the effects of varying the size of the steel section and the amount of longitudinal slab reinforcement on the behavior of composite beams in an isolated negative moment region. Twelve beams were tested with varying amounts of reinforcement in combination with 3 different steel sections. The beams were tested to failure by applying a statically incremented load.

Failure of the beams was by local buckling of the web and compression flange.

The results of these tests indicate that for a given steel section significant increases in the ultimate moment capacity in negative bending can be achieved by the addition of longitudinal slab reinforcement. However, this increase is accompanied by a significant reduction in the rotation capacity of the negative hinge. These tests also indicated that the increase in ultimate moment is not directly proportional to the increase in theoretical plastic moment values.

ACKNOWLEDGEMENTS

This investigation was made possible through financial assistance provided by the National Research Council of Canada.

The author wishes to extend his sincere thanks to Professor J. Longworth for his guidance during the testing program and in the preparation of this report.

The author also wishes to thank Mr. H. Panse and staff of the Department of Civil Engineering, and others who assisted in the fabrication and testing of the beam specimens.

TABLE OF CONTENTS

PAGE

LIST OF TABLES

LIST OF PLATES

LIST OF FIGURES

PAGE

NOMENCLATURE

A_c	area of concrete in slab
As	area of longitudinal slab reinforcement
A_t	area of transverse slab reinforcement
A_{WF}	area of wide flange section
b	width of flange
d	depth of steel section
F_Y	yield stress of longitudinal slab reinforcement
h	clear depth of web
M	moment
M_P	theoretical simple plastic moment for composite section
$M^o{}_P$	theoretical simple plastic moment of steel section
M_{ULT}	ultimate moment for composite section
$M^o{}_{ULT}$	ultimate moment of steel section
P_{ULT}	ultimate load
t	thickness of flange
w	thickness of web
ϕ_{ULT}	curvature at ultimate moment
θ_{ULT}	rotation at ultimate moment

CHAPTER 1

INTRODUCTION

1.1 INTRODUCTORY REMARKS

Since 1965, four investigations have been conducted in a study of continuous composite beams in the Department of Civil Engineering at the University of Alberta. The object of this study is to determine the behavior of composite beams over the full range of loading to failure and to propose design criteria based on ultimate load. The beams tested in this study consisted of rolled sections of G40.12 steel connected by headed stud shear connectors to reinforced cast-in-place concrete slabs.

In recent years, continuous composite beams have been used in bridge and building construction. The ability of composite beams to resist positive moments is well known. But to date, their behavior in negative bending is not as well understood. Some design specifications such as the American Association of State Highway Officials "Standard Specifications for Highway Bridges," 1965, and the British Code of Practice for Composite Construction in Structural Steel and Concrete, CP 117, allow consideration of the longitudinal slab reinforcement in the computation of the moment of inertia in a region of negative bending, while the current Canadian Standards Association Standard S16, 1965,

makes no reference to the negative moment region.

When designing structural steel flexural members, care is taken to prevent local buckling of the thin compression elements prior to attainment of the desired rotation capacity. This is also true for composite beams. In positive bending this presents little problem since the compression force in the slab reduces the depth of the steel section in compression, thereby reducing the probability of buckling. If adequate shear connectors are provided, the slab stiffens the compression flange of the steel section further restraining it from buckling. In negative bending, however, the concrete slab is connected to the tension flange. This places most of the steel section in compression, thereby increasing the tendency of the compression elements to buckle. The present investigation is concerned with the behavior of composite beams in negative bending, with emphasis on the effect of the size of the steel section on the rotation capacity of the composite section.

1.2 REVIEW OF PREVIOUS RESEARCH

1.2.1 GENERAL

The behavior of composite beams under positive moment is well known, but only recently have there been intensive investigations of composite beams subject to negative bending. Two investigations in the present University of Alberta study, by Piepgrass [(2)] in 1968 and

Davison[1] in 1969, have studied an isolated negative moment region. Isolated negative moment regions of composite beams have also been studied at the University of Cambridge.

1.2.2 RESEARCH AT THE UNIVERSITY OF CAMBRIDGE

Since 1960, several studies have been conducted at the University of Cambridge to determine the behavior of composite beams. The chief aim of these investigations was to develop ultimate strength design methods for continuous composite floor structures such as high-rise buildings and multi-deck bridge structures. The initial investigation was conducted by Barnard and Johnson[6]. Six simply supported composite beams with flange width to thickness ratios below 4.8 were subjected to positive bending. On the basis of observed material properties of steel and concrete, the results of a computer analysis agreed closely with the experimental results. Design rules were then established and checked against 63 computer analyses.

The results of this investigation suggested that elastic theory gave accurate predictions of flexural rigidity and curvature at first yield, but the bending moment at yield was overestimated by 13 percent. This was due to the presence of shrinkage and residual stresses in the specimen. If full plasticity of the steel section was assumed, the error in the ultimate moment rarely exceeded 5 percent. However, curvature at ultimate load was influenced by the shape of the stress-

strain relationship for concrete, consequently it could not be predicted accurately.

Four continuous beams with narrow concrete flanges were also tested. High-yield longitudinal reinforcement produced a force in the longitudinal slab reinforcement at yield in tension of 0.25 to 0.70 times the force in the rolled steel section at yield in compression. Shear connectors were uniformly spaced along the member. The results of these tests showed that the moment-curvature relationship in negative bending agreed closely with theoretical curves until large curvatures were reached and secondary failure occurred. Strain hardening caused overloading of shear connectors, resulting in more slip and increased deflection than encountered in the simple beam tests.

In 1966, van Dalen[9,10] conducted tests on simple composite beams which simulated the negative moment region of a continuous beam. In 8 of the tests the steel section was continuous over the length of the beam and the load was applied as a point load to the compression flange at midspan. In 5 of the tests, 2 typical beam column connections and a short column stub were introduced. A uniform distributed load was applied to the slab by 24 equal point loads. The steel section used was a 3 in. x 5 in. I section. The width of the slab varied from 12 in. to 30 in. and the ratio of the force in the longitudinal slab reinforcement at yield to the force in the steel section at yield ranged from .19 to .63.

Several modes of failure were observed. These consisted of crushing of the bottom surface of the concrete slab, longitudinal splitting, buckling of the column stub web, shear failure in the slab and buckling of the compression flange. The behavior of a wider variety of beam cross sections was studied in 49 computer analyses.

The results of this investigation indicated that if adequate shear connectors and transverse reinforcement are provided, the resistance to bending in the negative moment region with longitudinal slab reinforcement continues to increase with curvature until buckling occurs in the steel section, even though the slab is cracked in tension. Reliable predictions of the observed longitudinal strains, curvature, and rotations at all loads up to ultimate may be obtained if complete interaction and plane sections are assumed.

1.2.3 RESEARCH AT THE UNIVERSITY OF ALBERTA

In 1968, Piepgrass (2) studied behavior of composite beams in negative bending. Six beams representing an isolated negative moment region were tested. The main variables in the investigation were the amount of longitudinal reinforcement and the slab width. Four beams had a slab width of 3'-0" and amounts of longitudinal reinforcement ranging from 1.20 to 3.10 sq. in. Three beams each with an area of longitudinal reinforcement equal to 2.48 sq. in. had slab widths varying from 3'-0" to 5'-0". A slab thickness of 3 in. was used for all the beams. The

steel section in all beams was a 12 B 16.5 having width to thickness ratios of 7.43 for the compression flange and 46.7 for the web. However, in order to avoid premature local flange buckling, the compression flange of 4 beams was stiffened by a 3 in. x 3/8 in. steel plate. This decreased the width to thickness ratio of the compression flange to 6.0.

The beams without cover plates failed in local buckling of the flange and web. Those with cover plates failed in lateral buckling. Due to the low rotation capacity of these beams the ratio of the ultimate moment to the computed simple plastic moment was low, ranging from .98 to 1.07.

It was concluded that ultimate capacity increased with increase in longitudinal reinforcement. However, the average stress in the longitudinal reinforcement at ultimate did not reach the yield stress. A steel section, defined as compact under the provisions of Canadian Standards Association Standard S16, did not necessarily provide adequate rotation capacity for the formation of a plastic hinge in a composite beam in negative bending.

The next investigation within the University of Alberta study was conducted by Davison(1) in 1969. The object of this investigation was to study further the effect of longitudinal slab reinforcement on rotation capacity. A secondary objective was to further study the effects of varying slab width. A total of 8 beams were tested. BEAMS 11 to

14 were designed to indicate the effect of amounts of longitudinal reinforcement ranging from 1.18 sq. in. to 3.68 sq. in. on the rotation capacity of the section. These 4 beams had a slab width of 4'-0". BEAMS 15, 16, and 17 were designed to show the effects of varying the width of slab from 2'-8" to 6'-0". BEAMS 16 and 17 had 2.45 sq. in. of slab reinforcement and BEAM 15 had 3.68 sq. in. of slab reinforcement. All slabs were 4 in. thick. The 12WF36 steel section used in all beams had width to thickness ratio of the compression flange and web of 6.07 and 34.0 respectively. Sufficient shear connectors were provided to withstand the force in the longitudinal reinforcement at yield and were spaced uniformly throughout the span.

After sufficient rotation had occurred for a negative hinge to form, the beams failed in local buckling of the web and compression flange. Lateral buckling was prevented by the use of lateral braces at the load and reaction points. In all beams, points on the unloading portion of the load-deflection curve were obtained. The ratio of the experimental ultimate moment capacity to the theoretical simple plastic moment capacity ranged from 1.20 for the beam with the largest amount of longitudinal reinforcement to 1.35 for the beam with the least amount of reinforcement.

It was concluded that the addition of longitudinal slab reinforcement significantly increases the ultimate negative moment capacity of composite beams, but the increase

is not proportional to the increase in the simple plastic moment values. The rotation capacity of the negative moment sections decreased as the amount of longitudinal slab reinforcement increased. For a given amount of reinforcement, variation in slab width, within the limit permitted by Canadian Standards Association Standard S16, had no significant effect on ultimate moment capacity or rotation capacity. When buckling of the steel section did not occur, the longitudinal slab reinforcement reached yield conditions prior to ultimate moment. However, the corresponding curvature was greater than that predicted from the linear strain distribution across the steel section.

1.3 SCOPE OF PRESENT INVESTIGATION

The primary objective of the present investigation is to study the effects of varying the size of the steel section on the behavior of composite beams in an isolated negative moment region. A secondary objective is to further study the effect of longitudinal slab reinforcement on the behavior.

CHAPTER II

TEST PROGRAM

2.1 DESIGN OF TEST SPECIMENS

2.1.1 CHOICE OF STEEL SECTIONS

The main requirement of the steel sections was that they be compact as defined by CSA Standard S16. The steel section in a composite member in negative bending may be considered as a steel beam under combined axial load and bending. Therefore, the clear depth to thickness ratio of the web elements under compression is limited to $\frac{255}{\sqrt{Fy}}$ and the width to thickness ratio of the projecting elements of the compression flange is limited to $\frac{54}{\sqrt{Fy}}$ to prevent premature local buckling. As in previous investigations at the University of Alberta, CSA G40.12 material was used, therefore the limiting width to thickness ratios are 40.3 for the web and 8.54 for the flange.

The 12WF36 section used in Davison's (1) investigation has width to thickness ratios of 34.0 for the web and 6.07 for the flange, and possesses appreciable rotation capacity. On the other hand, the 12B16.5 section used in Piepgrass' (2) investigation with width to thickness ratios of 46.7 and 7.43

respectively had very limited rotation capacity in negative bending. The slenderness of the section resulted in lower resistance to local buckling. In the present investigation, sections between those used by Davison and Piepgrass, were chosen.

2.2 FABRICATION OF TEST SPECIMENS

The steel sections were fabricated by Canron Limited of Edmonton from CSA G40.12 material. Most beams of the same size were from the same heat lot; however, two additional 12WF31 sections and one 12WF27 section, ordered at a later date, were from different heat lots. Fabrication included the attachment of round headed shear connectors along the centerline of the beam, bearing stiffeners at support and load points, lugs over the supports and a pin at midspan on the compression flange for the lateral bracing. After testing one composite and one plain beam, it became evident that additional stiffeners were required in the region between the load points to ensure that failure due to local buckling would occur outside this region. Additional stiffeners were welded in place by University of Alberta Technical Services. One additional pair of stiffeners was provided on the WF sections and two pairs on the 12B16.5 sections. Care was taken to ensure that additional welding did not deform the beams; however, slight warping could not be prevented. The steel sections were ground smooth at strain gage locations

on the webs and flanges before placing in prefabricated wood forms for the casting of the concrete slab. FIGURE 2.1 shows the details of the fabricated steel section.

The slab reinforcement was prepared by tying the transverse and longitudinal bars into mats and then grinding the bars smooth at the 6 gage locations. Styrofoam blocks were taped to the bars at these locations so that the bars could be easily exposed after the concrete hardened. Plastic chairs were used to hold the reinforcement in place prior to casting the concrete. Plate 2.1 shows the fabricated steel specimen and the reinforcing mats in position prior to casting.

The concrete for the slabs was batched at the University of Alberta Structural Engineering Laboratory in a 9 cubic foot Eirich mixer. The slump ranged from 3 1/4 in. to 3 3/4 in. Two batches were required for each slab from which 6 test cylinders were taken. The concrete was vibrated into place using a mechanical vibrator and was leveled with a wooden screed and steel trowel. Curing of the concrete was under laboratory conditions for periods ranging from 22 to 75 days. The composite beams were removed from the forms at 7 days after which time, the electrical resistance SR4-A7 strain gages were installed.

2.3 PROPORTIONING OF THE COMPOSITE SECTION

All composite sections consisted of a 4 in. thick concrete slab, 4'-0" in width. The total length of each

specimen was 10'-0". Of this 1'-0" at each end was used to anchor the slab reinforcement resulting in a span length of 8'-0".

2.4 LONGITUDINAL SLAB REINFORCEMENT

From previous investigations it was evident that increasing the longitudinal slab reinforcement above the amount required to place the neutral axis into the tension flange does not increase the ultimate capacity of the section significantly. Therefore, the ratio of the longitudinal reinforcement to the area of the steel section was kept below .382. Several different $\frac{A_s}{A_{WF}}$ ratios were used for each of the 3 test series to indicate the effect of varying the amount of longitudinal reinforcement on the rotation capacity of the section. BEAMS 22 and 32 had $\frac{A_s}{A_{WF}}$ ratios of approximately .10, BEAMS 23, 33, and 42 had ratios of approximately .20, and BEAMS 24, 25, 34, and 43 had ratios from .27 to .38 placing the neutral axis in the tension flange at ultimate load. Three plain beams, one of each size, were tested as BEAMS 21, 31, and 41 to provide a basis for comparison. TABLE 2.6 describes the test specimens. FIGURE 2.2 shows a typical cross section of the composite beams.

2.5 MATERIAL PROPERTIES

The concrete properties are summarized in TABLE 2.1. Two cylinders from each slab were tested at 7 or 8 days and the remaining 4 cylinders were tested on the day of the

beam test.

Results of tensile tests performed on the structural steel are shown in TABLES 2.2, 2.3 and 2.4. The tensile coupons were cut, 2 from the web and 2 from each flange, from 3'-0" lengths supplied with the fabricated beams. Results of tension tests performed on 22" lengths of #3, #4, and #5 reinforcing bars are shown in TABLE 2.5.

2.6 INSTRUMENTATION

Strains in the slab reinforcement and steel sections were measured by means of SR4-A7 electrical resistance strain gages. All reinforcement mats, except one, had 6 gage locations, 4 on the longitudinal bars and 2 on the transverse bars. The gages on the longitudinal bars were located at midspan of the beam, on the 2 innermost and 2 outermost bars. The gages on the transverse reinforcement were located on 2 bars at midspan. BEAM 32 had 4 additional gages on the innermost longitudinal bars, 2 over each support. Locations of gages on reinforcing bars are shown on FIGURE 2.3.

The number of strain gages on the steel section varied from 4 to 14. On each beam 4 gages were located on the flanges 1 in. from the tip (1/2 in. for the 12B16.5). BEAMS 22, 24, and 33 had no strain gages on the web. On BEAMS 21 and 41, ten gages were located on the web, 5 on either side. BEAMS 42 and 43 had 8 gages on the web, 4 on either side. The remaining beams had 9 gages on the web, 4 on one side and 5 on the other. Strain gage locations

on steel sections are shown in FIGURE 2.4

Beam deflection at midspan was measured using Mercer Dial Gages having an accuracy of $\pm$ .001" and a free travel of 2 in. Two gages measured deflections of the concrete slab, 2 in. from the slab edges and the other 2 measured deflections of the tension flange of the steel section. Each dial gage was supported by a magnetic base on a steel channel connected to the loading frame. As the ultimate load was reached, the slab began to deflect so quickly that the deflection gages ran out of travel before they could be reset, therefore, deflections were measured using a precise level and a steel scale suspended from the midpoint of the slab.

Rotations of the test specimens were measured at the supports and at each load point. At the supports, both mechanical and electrical rotation meters were used, while at the load points only electrical rotation meters were used. The mechanical rotation meters were bolted rigidly to the beam web, one at each end of the beam. These meters consisted of a level tube, an extension dial, and two arms connected by a hinge. At each load increment the hinged arm was re-levelled using the extension dial. From the extension dial reading and the pivot length of the two arms the rotations were obtained. The electrical rotation meters measured rotations in the form of bending strains induced in a thin strip of metal from which a large weight was suspended. The strip was fixed between the weight and a connecting plate which was rigidly

bolted to a bracket welded on the test specimen at the point where the rotation was required. As the beam rotated, the weight remained vertical inducing bending strains in the thin steel strip which were measured on a strain indicator. The relationship between strain and rotation had been previously determined by calibrating the rotation meter.

Two Mercer Dial Gages with a free travel of 1 in. and an accuracy of $\pm.001''$ were used to indicate the occurrence of local buckling of the compression flange near the load points. Two similar dial gages were fixed to the supporting concrete pedestals to measure the relative horizontal movement of the supports as the beam deflected. Slip between the concrete and the steel was recorded on dial gages at each end of the beam. FIGURE 2.5 shows the location of the instrumentation on the specimens. PLATE 2.2 shows a typically instrumented beam.

2.7 DESIGN OF TESTING EQUIPMENT

2.7.1 DESIGN OF ARTICULATED LATERAL BRACE

From previous investigations by Davison and Piepgrass, it was evident that lateral bracing should be employed to ensure lateral stability of the test specimens. Tie rods were used to brace the compression flange at the supports and an articulated brace was employed at midspan. The articulated brace was designed to support the compression flange laterally, while allowing the beam to deflect. This was made possible

by using ball and socket joints at each end of two turnbuckles.

The end tie rods were connected to lugs welded on the compression flange, while the articulated midspan brace swivelled about a pin or bolt welded on the compression flange. Details of the lateral bracing system are shown on FIGURE 2.6

2.7.2 TESTING EQUIPMENT

The composite specimens were tested with the slab on the underside and load was applied by a single 220 kip Amsler Jack bearing on a loading bridge which distributed the total load as two loads 5 in. on either side of midspan. The jack reacted against a beam supported by four columns anchored to the load bed. The jack had a free travel of 5 in. which was never exceeded during this investigation. Details of the testing equipment are shown in FIGURE 2.6 and PLATE 2.3.

The test specimens were supported at each reaction point on a concrete pedestal on which was seated a 1 in. steel plate and a 12 in. roller unit fitted with a rocker plate assembly. Only one roller was free to move longitudinally.

2.8 TESTING PROCEDURE

Prior to testing, the test specimen was lifted onto the rocker plates and seated in plaster of Paris. The electrical rotation meters were bolted to supporting brackets and connected, as were the strain gages, to a strain indicator.

Mechanical rotation meters were bolted to the beam web, and the dial gages were positioned.

A load of 1 kip was applied and removed before recording initial readings. Shrinkage cracks in the concrete were marked at this time.

The load was applied in increments of 10 kips until the deflection rate began to increase due to yielding. The size of further load increments was based mainly on deflection considerations. At each load increment, after allowing some time for the beam to stabilize, readings were recorded and cracks in the concrete slab were marked. At first evidence of web buckling, the load maintainer on the Amsler Jack was released and further loading was maintained manually. This made it possible to control the load during the unloading stages. In order to obtain the readings for the unloading portion of the load deflection curve, the load was reduced manually until conditions stabilized sufficiently long enough to permit readings.

The test terminated when the jack was fully extended or when local buckling caused the jack to rotate. All specimens, except BEAM 21, were tested well into the unloading range and exhibited large flange and web local buckles.

Due to some twisting in most of the tests, metal shims were required under the loading bridge to maintain a vertical load. Therefore, during the course of a test, the specimen was unloaded, shims inserted as required, and

load re-applied. In some cases the shimming operation was repeated several times during the course of the test.

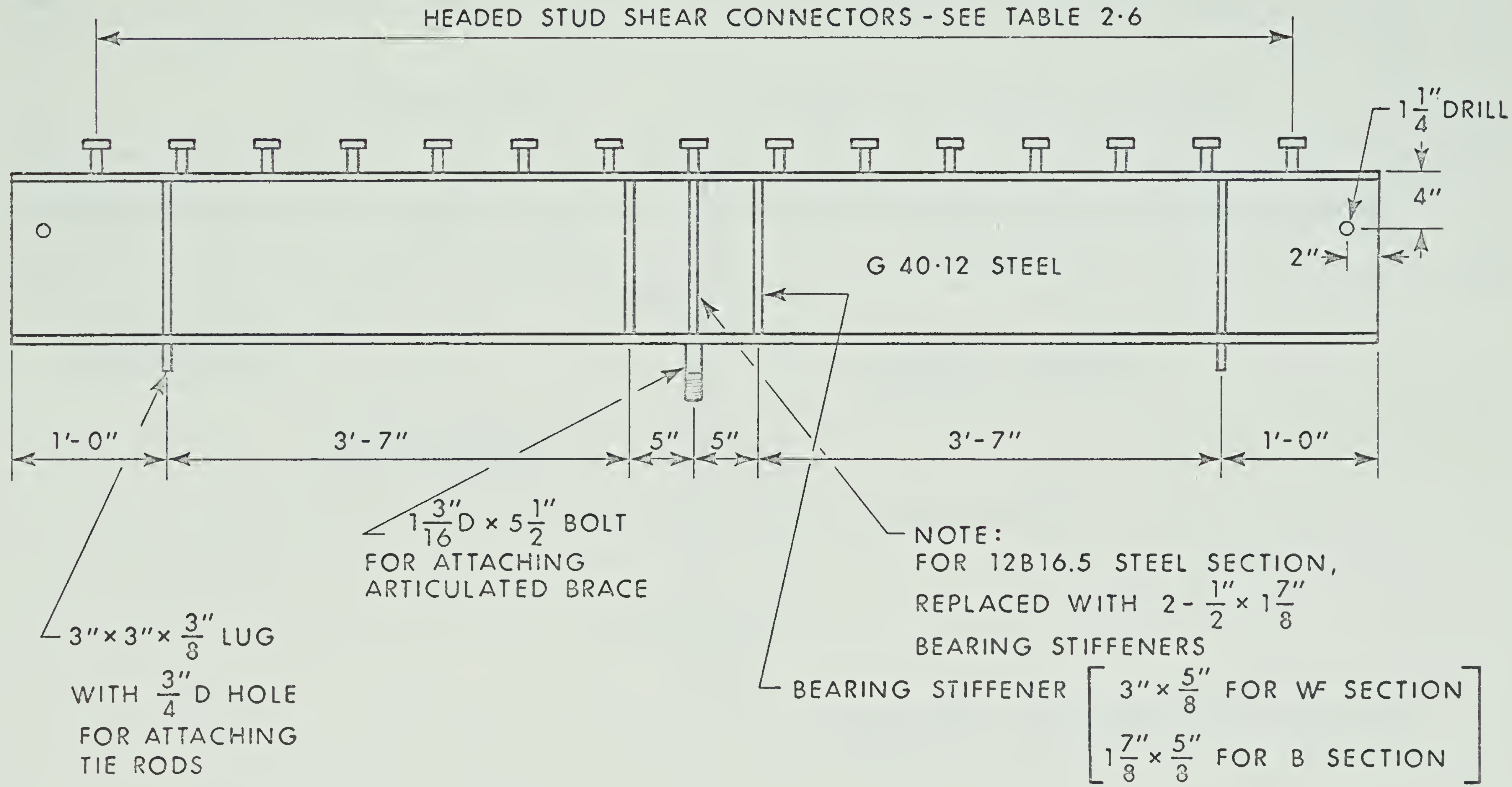

FIGURE 2·1 FABRICATED STEEL SECTION

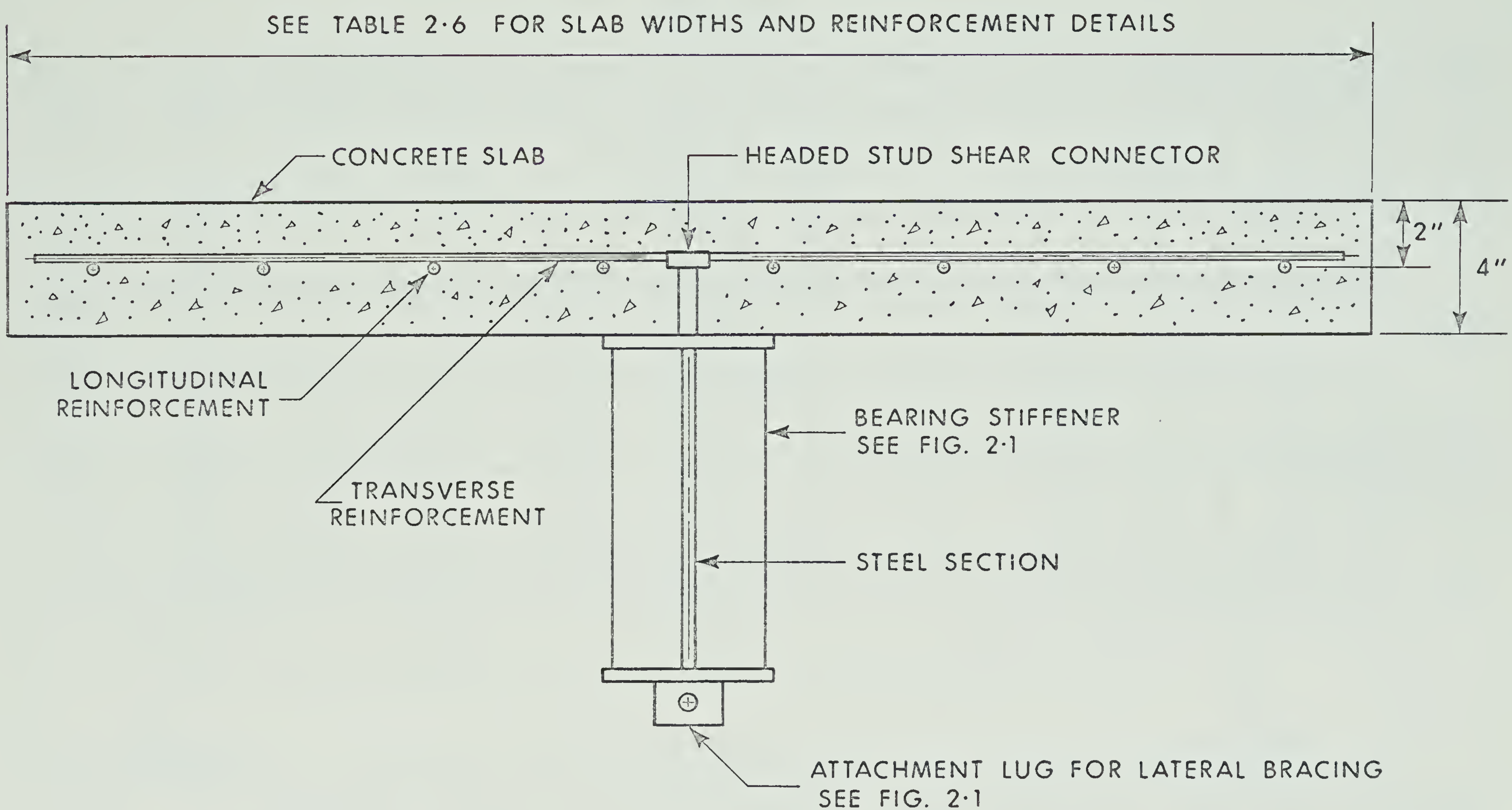

FIGURE 2·2 COMPOSITE BEAM CROSS SECTION

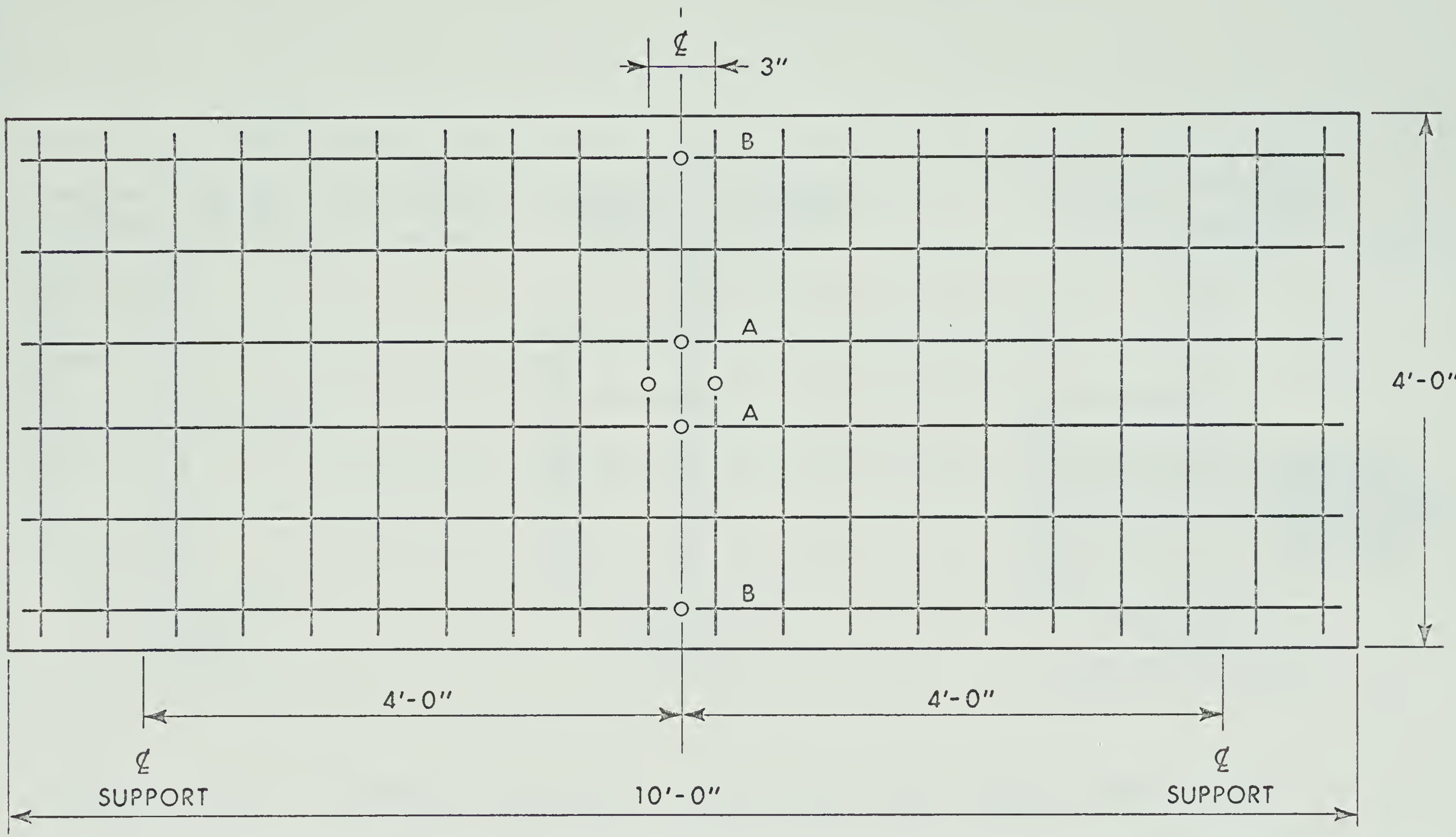

NOTE: THE ARRANGEMENT SHOWN IS FOR BEAMS 23 AND 43. THE NUMBER AND ARRANGMENT OF BARS DIFFERS FOR OTHER BEAMS.

FIGURE 2·3 TYPICAL STRAIN GAUGE LOCATIONS ON SLAB REINFORCEMENT

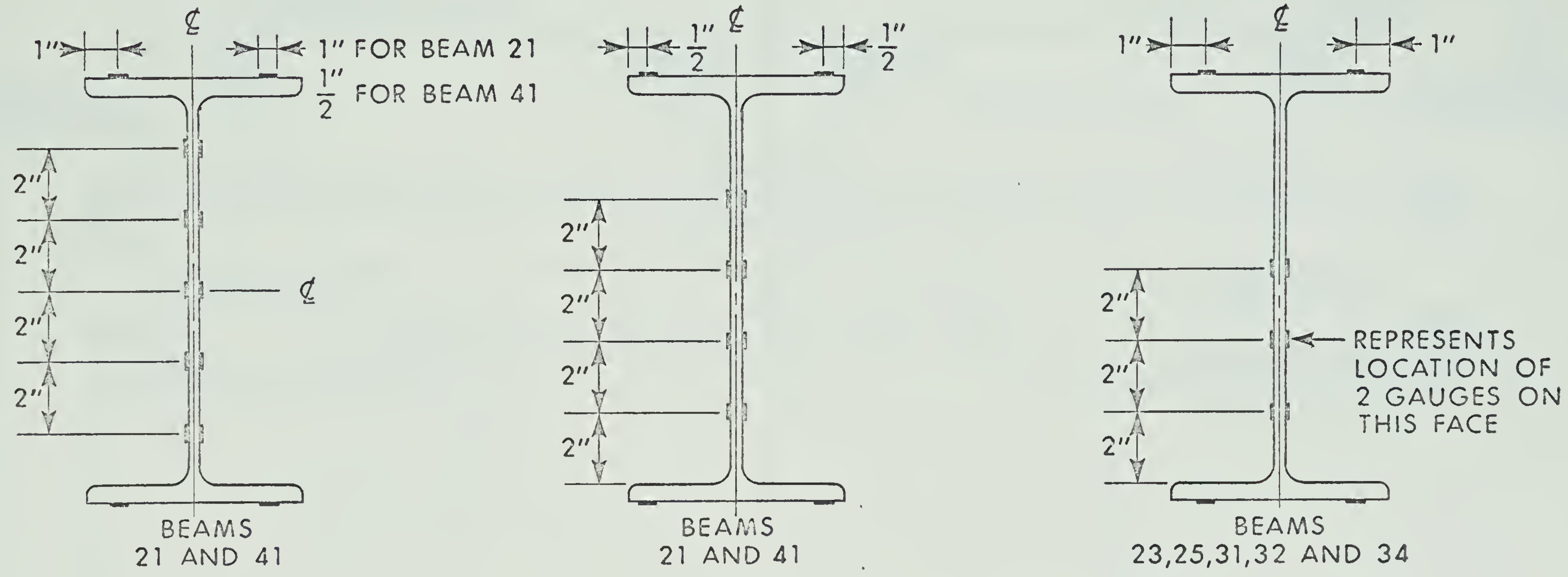

FIGURE 2·4 STRAIN GAUGE LOCATION ON STEEL SECTIONS

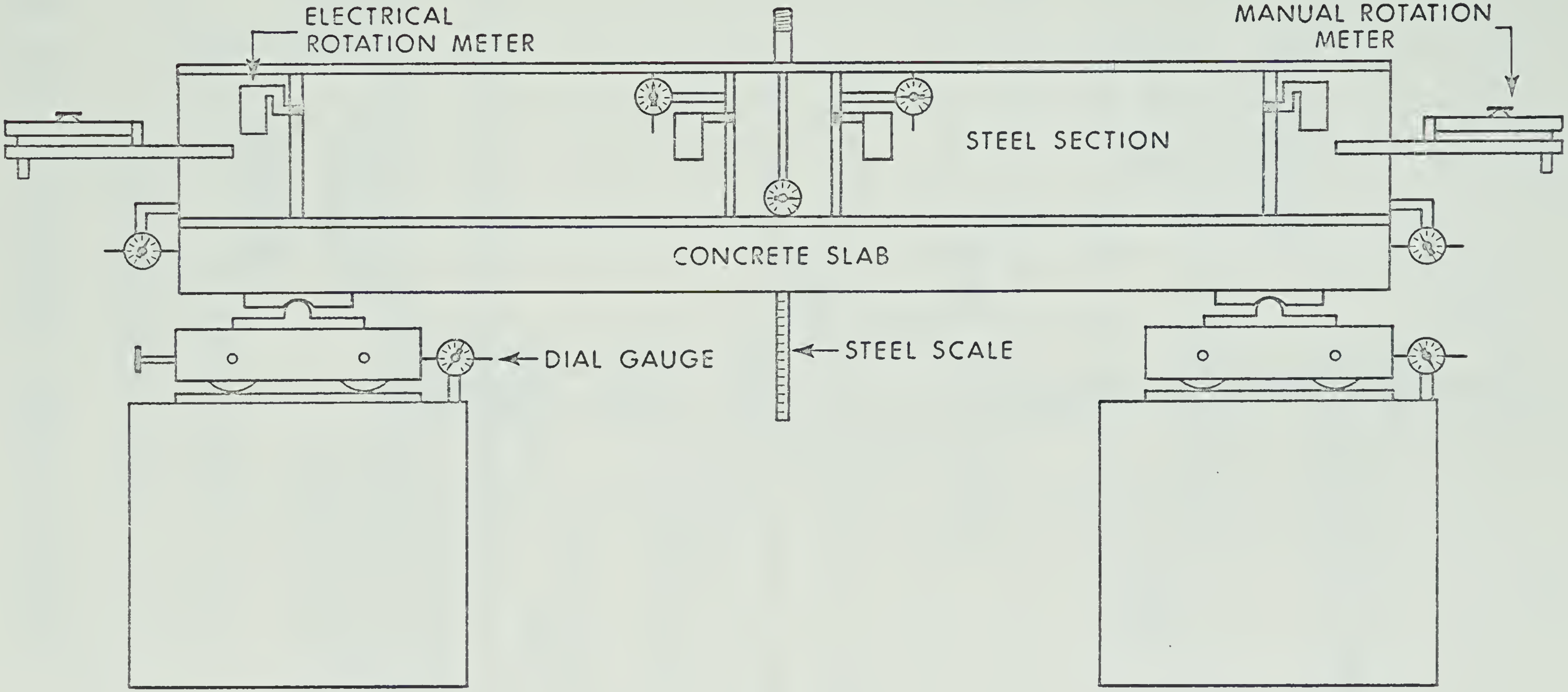

ELEVATION VIEW

FIGURE 2·5 INSTRUMENTATION

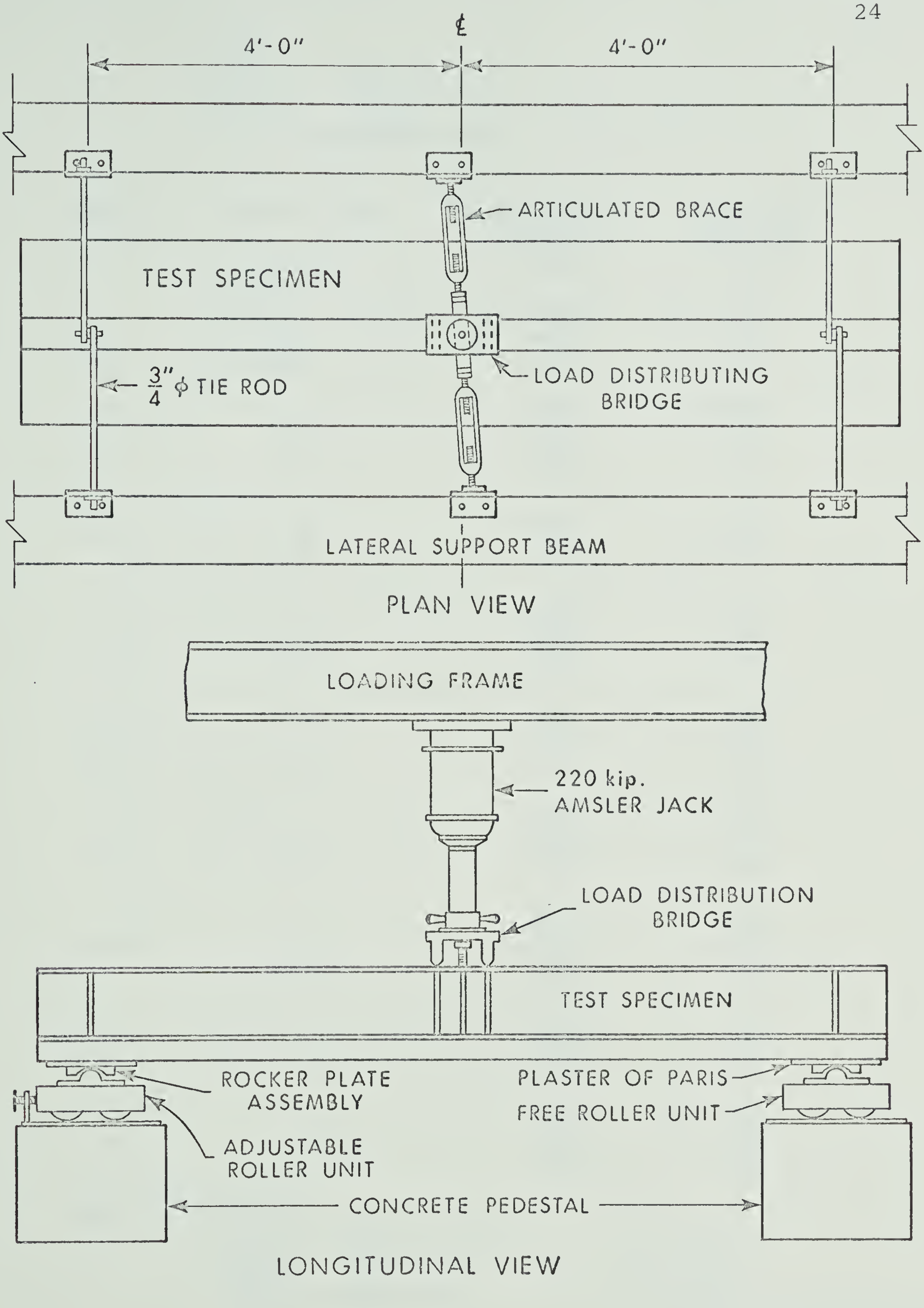

FIGURE 2·6 TESTING ARRANGEMENT

TABLE 2.1

CONCRETE DATA

BEAM	AGE AT TEST (days)	COMPRESSIVE STRESS (psi)	SPLITTING TENSION (psi)
	8	3640	666
22	49	4060	610
	49	4200	666
	7	3180	618
23	73	3220	403
	73	3220	375
	8	3920	700
24	39	4540	674
	39	4710	660
	8	2880	600
25	24	3280	618
	24	3340	615
	8	2350	340
32	22	2760	348
	22	2500	400
	8	2860	626
33	44	4140	610
	44	4000	650
	7	2800	368
34	66	3660	528
	66	3180	444
	7	3380	543
42	75	4030	598
	75	4380	472
	7	3200	514
43	67	3730	646
	67	3780	630

MIX PROPORTIONS

Cement (high early)	133 lbs.
Sand	344 lbs.
Coarse Aggregate	500 lbs.
Water	80 lbs. (approximately)

Slump 3 1/2"

TABLE 2.2

12WF 31 MATERIAL PROPERTIES

COUPON LOCATION		YIELD STRESS (ksi)	ULTIMATE STRESS (ksi)	MODULUS OF ELASTICITY (ksi)	STRAIN AT STRAIN HARDENING (in/in)	STRAIN HARDENING MODULUS (ksi)
FLANGE		40.7	69.4	33600	0.0111	722
		41.7	69.6	27800	0.0086	827
		41.0	70.0	29300	0.0115	744
	Ave.	41.1	69.7	30200	0.0104	764
WEB		47.0	72.5	33600	0.014	783
		46.4	70.2	32200	0.0156	788
	Ave.	46.7	71.3	32900	0.0148	785

TABLE 2.3

12WF 27 MATERIAL PROPERTIES

COUPON LOCATION		YIELD STRESS (ksi)	ULTIMATE STRESS (ksi)	MODULUS OF ELASTICITY (ksi)	STRAIN AT STRAIN HARDENING (in/in)	STRAIN HARDENING MODULUS (ksi)
FLANGE		48.7	77.2	34700	0.0086	790
		47.8	77.9	29900	0.0060	553
		47.7	79.8	39800	0.0079	805
		49.4	77.0	30800	0.0080	725
	Ave.	48.4	78.0	33800	0.0076	718
WEB		53.8	79.3	38500	0.0158	725
		52.7	78.0	42000		712
		53.3	78.6	40250	0.0158	718

TABLE 2.4

12B16.5 MATERIAL PROPERTIES

COUPON LOCATION	YIELD STRESS (ksi)	ULTIMATE STRESS (ksi)	MODULUS OF ELASTICITY (ksi)	STRAIN AT STRAIN HARDENING (in/in)	STRAIN HARDENING MODULUS (ksi)
FLANGE	43.8	68.0	29200	0.0154	734
	44.9	68.6	28100	0.0160	580
	46.2	68.1	28900	0.0162	553
	45.4	68.1	25200	0.0150	507
	Ave.45.1	68.2	27800	0.0157	593
WEB	46.4	69.1		0.0186	652
	48.8	69.8	28700	0.0226	580
	Ave.47.6	69.5		0.0206	616

TABLE 2.5

SLAB REINFORCEMENT DATA

TYPE	YIELD STRESS (ksi)	ULTIMATE STRESS (ksi)
#3	53.2	79.6
	52.7	76.0
	51.8	76.3
	52.2	77.6
	50.9	75.9
	51.3	76.4
	Ave. 52.0	77.0
#4	49.0	72.3
	47.8	73.0
	46.5	73.8
	50.0	73.8
	50.0	72.5
	47.5	73.8
	Ave. 48.5	73.2
#5	51.7	77.3
	51.4	76.8
	51.7	77.4
	48.7	77.0
	47.7	76.6
	50.2	77.0
	Ave. 50.7	77.0

TABLE 2.6

TEST SPECIMENS

BEAM NUMBER	STEEL SECTION	SLAB WIDTH	LONGITUDINAL REINFORCEMENT	As (sq.in.)	$\frac{As}{A_{WF}}$	$\frac{As}{A_c}$	SHEAR CONNECTORS	TRANSVERSE REINFORCEMENT	A_t/A_c
22	12WF31	4'-0"	4-#4	0.80	0.088	0.00417	3/4"øx3"@6"	#3 @ 6"	0.00458
23	12WF31	4'-0"	6-#5	1.86	0.204	0.00967	3/4"øx3"@6"	#3 @ 6"	0.00458
24	12WF31	4'-0"	8-#5	2.48	0.272	0.01290	3/4"øx3"@4½"	#3 @ 4½"	0.00612
25	12WF31	4'-0"	12-#5	3.72	0.408	0.01940	3/4"øx3"@4½"	#3 @ 4½"	0.00612
32	12WF27	4'-0"	4-#4	0.80	0.100	0.00417	3/4"øx3"@6"	#3 @ 6"	0.00458
33	12WF27	4'-0"	8-#4	1.60	0.201	0.00834	3/4"øx3"@6"	#3 @ 6"	0.00458
34	12WF27	4'-0"	10-#5	3.10	0.389	0.01620	3/4"øx3"@4½"	#3 @ 4½"	0.00612
42	12B16.5	4'-0"	2-#4,2-#5	1.02	0.208	0.00531	3/4"øx3"@6"	#3 @ 6"	0.00458
43	12B16.5	4'-0"	6-#5	1.86	0.383	0.00967	3/4"øx3"@6"	#3 @ 6"	0.00458

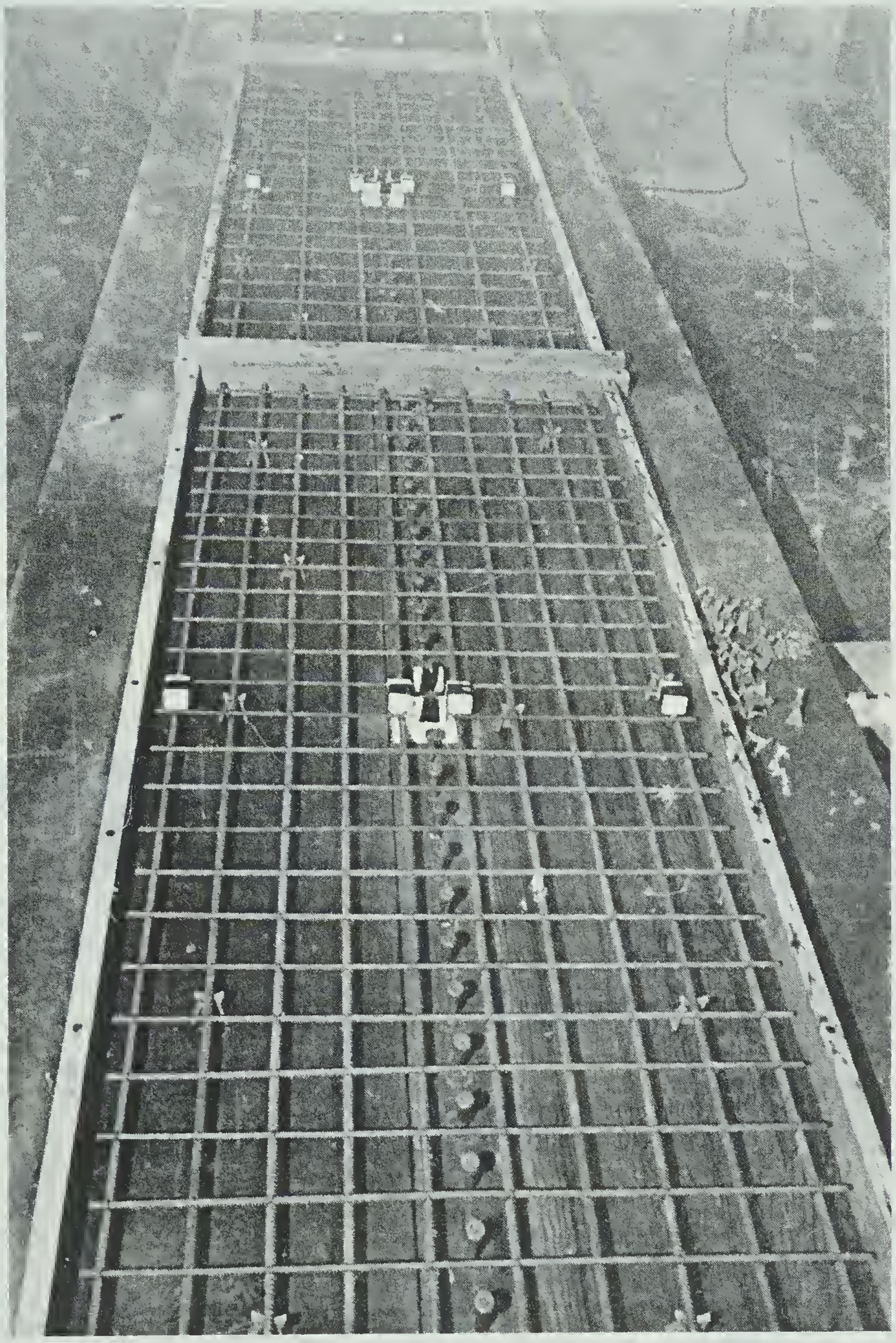

PLATE 2.1 12WF31 SPECIMENS PRIOR TO CASTING

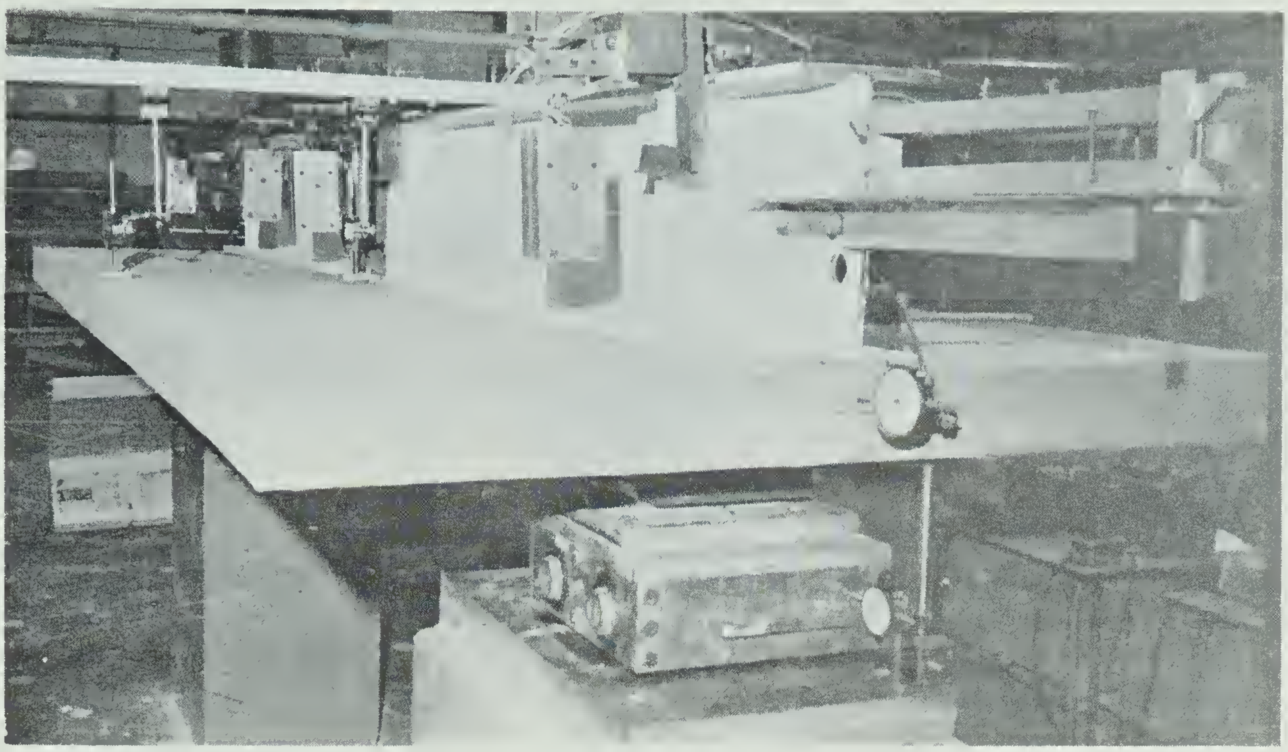

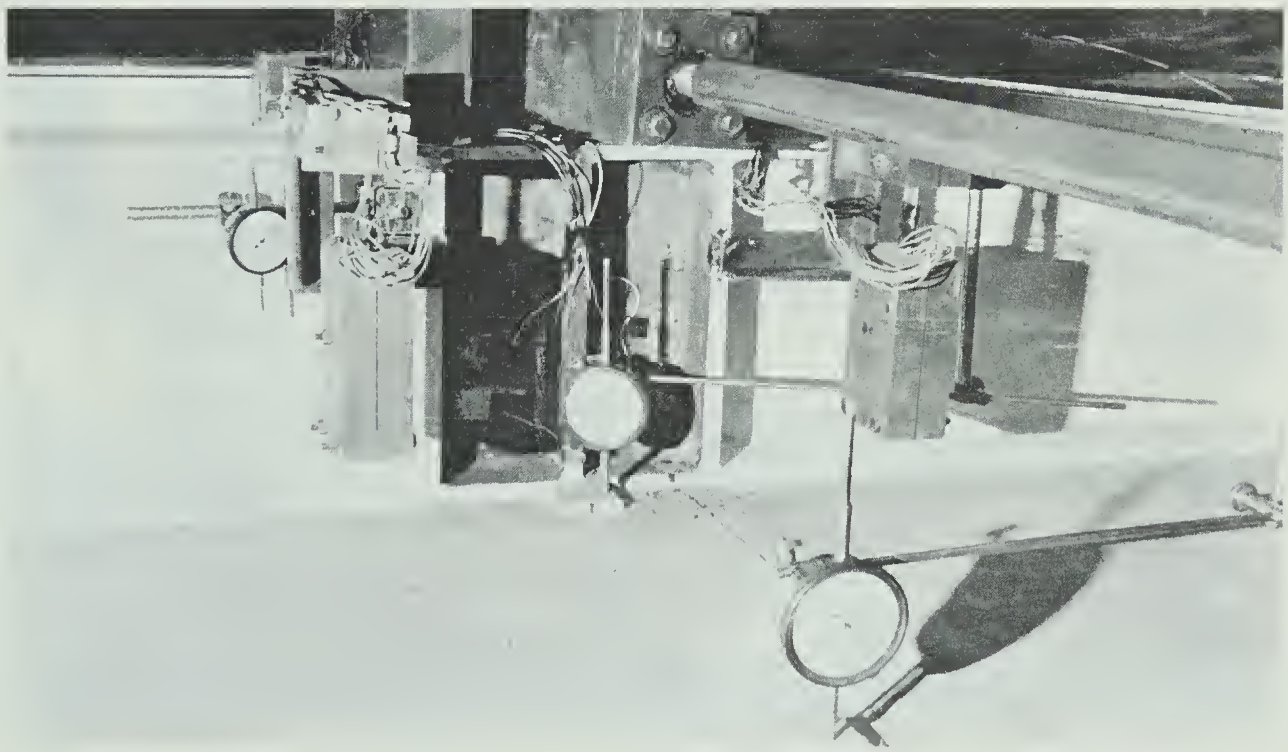

PLATE 2.2 INSTRUMENTATION

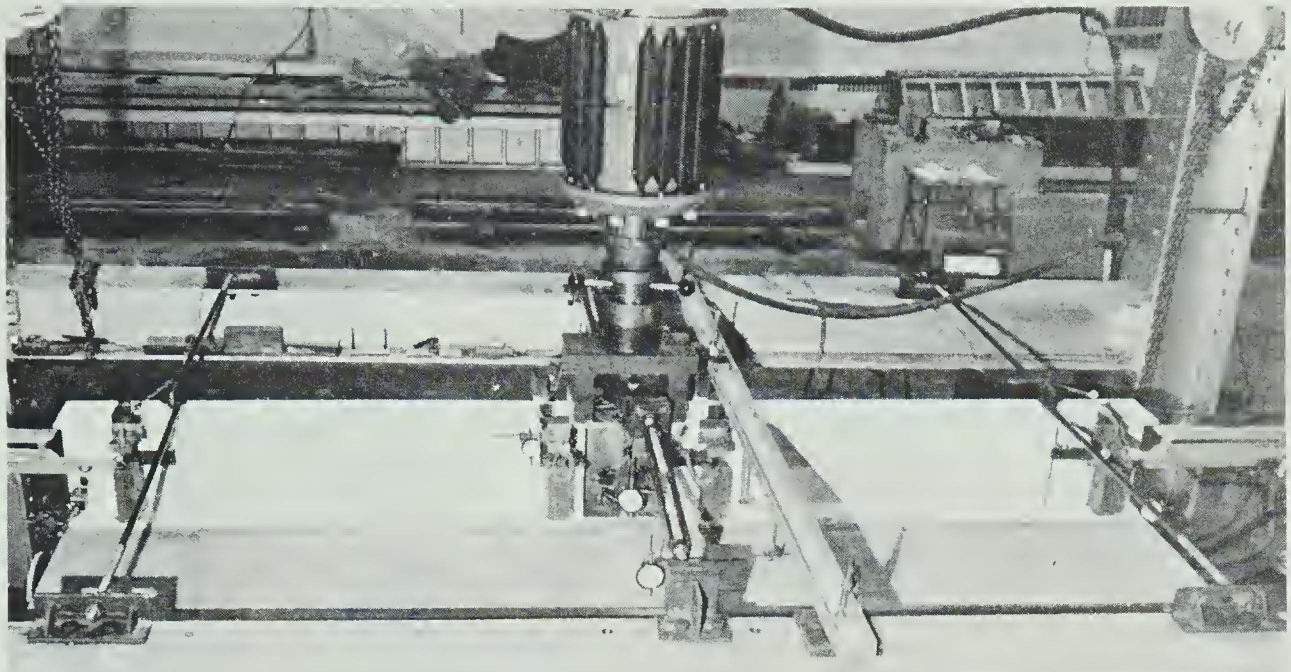

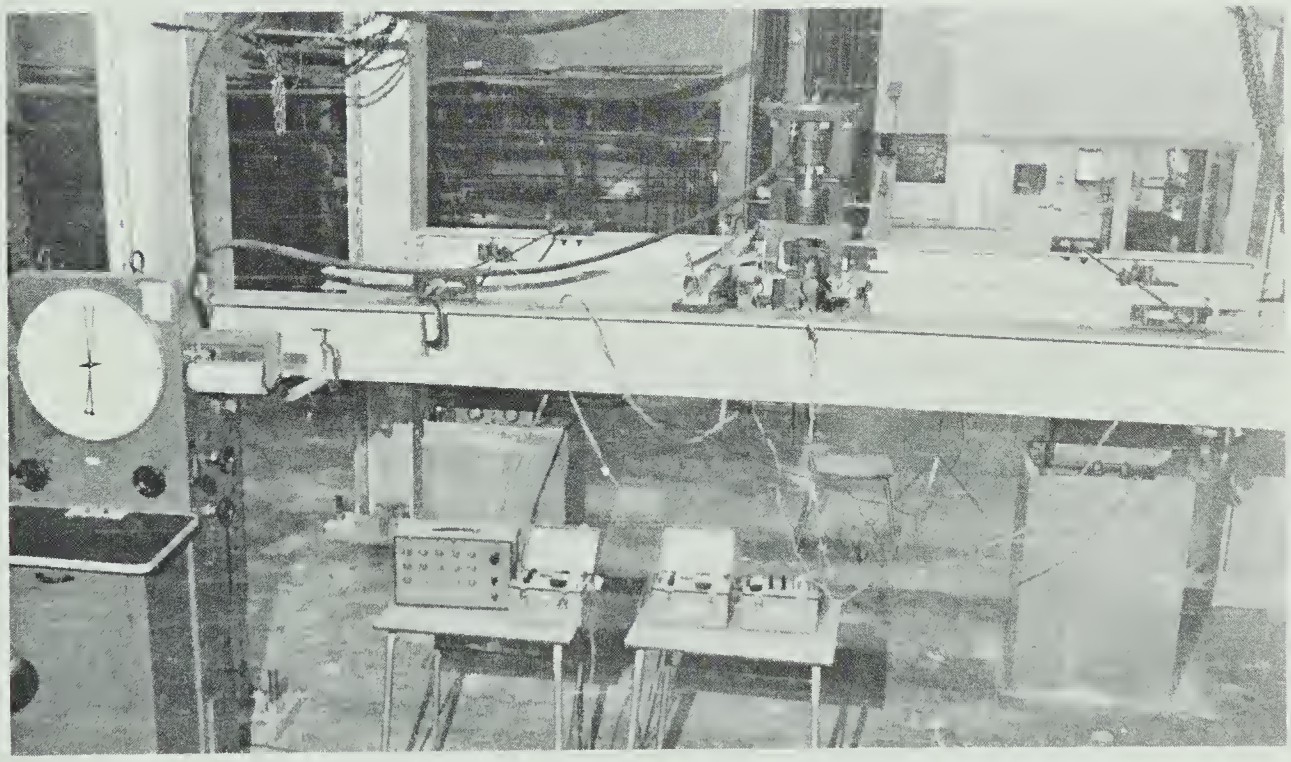

PLATE 2.3 TEST APPARATUS

CHAPTER III

TEST RESULTS

3.1 INTRODUCTION

The complete data obtained from the beam tests is filed in the Department of Civil Engineering at the University of Alberta. Most of the data is presented herein in graphic and tabular form.

3.2 LOAD-DEFLECTION RELATIONSHIPS

Load-deflection relationships are shown in FIGURES 3.1, 3.2 and 3.3. FIGURE 3.4 compares the load deflection relationships for composite beams of approximately the same $\frac{A_s}{A_{WF}}$ ratio but varying size of steel section. A comparison of the plain beams is shown in FIGURE 3.5.

3.3 MOMENT-CURVATURE RELATIONSHIPS

The midspan moment-curvature relationships are shown in FIGURES 3.6 to 3.8. Moment-curvature relationships for BEAMS 22, 24, and 33 are not presented since insufficient strain readings were taken to establish accurate curvature values. Moment-curvature relationships for the plain steel beams are shown in FIGURE 3.9 In FIGURE 3.10 the ratio of

actual moment to computed simple plastic moment $(\frac{M}{M_p})$ is used to nondimensionalize the moment scale and facilitate a comparison of curvatures for BEAMS 25, 34, and 43.

3.4 MOMENT-ROTATION RELATIONSHIPS

The relationship between the bending moment at mid-span and the total rotation of the beam, obtained by summing the two end rotations, is presented in FIGURES 3.11, 3.12, and 3.13. FIGURE 3.14 compares the rotation behavior of composite beams having similar $\frac{As}{A_{WF}}$ ratios but different size of steel section. Values of end rotations obtained from manual and electrical rotation meters were similar; therefore only the values obtained from the electrical rotation meters are presented.

FIGURES 3 15, 3.16, 3.17 and 3.18 present the relationships between the midspan bending moment and the rotation of a section located 5 in. from midspan of the beam on the end in which no local buckling occurred.

3.5 SLAB REINFORCEMENT STRAINS

Data obtained from the SR4-A7 strain gages located on the slab reinforcement is plotted in FIGURES 3.19, 3.20, and 3.21. FIGURES 3.19 and 3.20 present longitudinal bar strains at midspan. Each point represents the average for two bars symmetrically positioned.

In FIGURE 3.21 the relationships between applied load and transverse reinforcement strain at midspan are

presented. The points plotted are the average for the two transverse bars closest to midspan.

3.6 LOAD-SLIP RELATIONSHIPS

Load-slip curves for the test beams are shown in FIGURE 3.22. Points represent the sum of two slip measurements, one at each end of the beam.

3.7 SUPPORT MOVEMENT

The relative movement of the free roller support with respect to the fixed roller support is plotted against load in FIGURE 3.23.

3.8 ULTIMATE LOAD VALUES

TABLE 3.1 compares the theoretical simple plastic and experimental ultimate moment values. FIGURE 3.24 shows the variation in $\frac{M_{ULT}}{M_p}$ with respect to the total tensile force in the longitudinal slab reinforcement at yield for the beams in this investigation, and compares them with results obtained by Davison[1] and Piepgrass[2]. In FIGURE 3.25 the ratio of the ultimate moment of the composite section to the ultimate moment of the steel section is plotted against the total tensile force in the longitudinal slab reinforcement at yield for all the beams tested, together with BEAMS 11, 12, 13 and 14 of the previous investigation[1]. To compare the theoretical and experimental values, FIGURE 3.26 indicates the variation in the ratio of the calculated simple plastic moment

for the composite section to the simple plastic moment for the corresponding plain steel section with total tensile force in the longitudinal slab reinforcement for the same beams as above. The effect of varying parameters of the steel section on the ultimate capacity of composite beams with constant $\frac{As}{A_{WF}}$ ratios, is shown in FIGURES 3.27 and 3.28.

3.9 PLATES

In addition to the test results presented graphically, the behavior of the beams at failure is illustrated in several Plates. PLATE 3.1 shows the general deflected and buckled shape of the composite specimens. Views of typical load buckles and yield patterns at failure are shown in PLATE 3.2. The distribution of slab cracking is shown in PLATES 3.3. and 3.4.

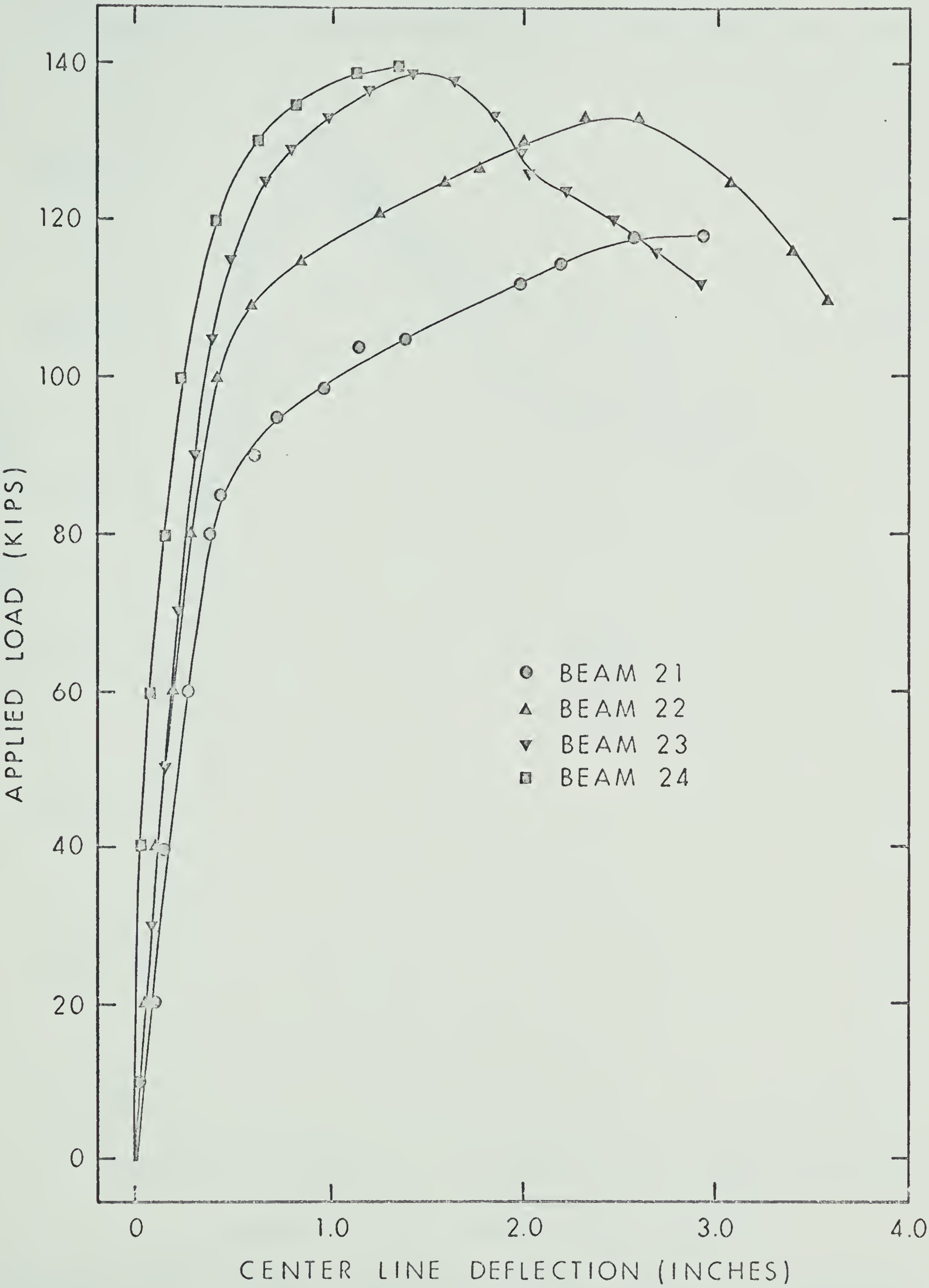

FIGURE 3.1 LOAD - DEFLECTION RELATIONSHIPS

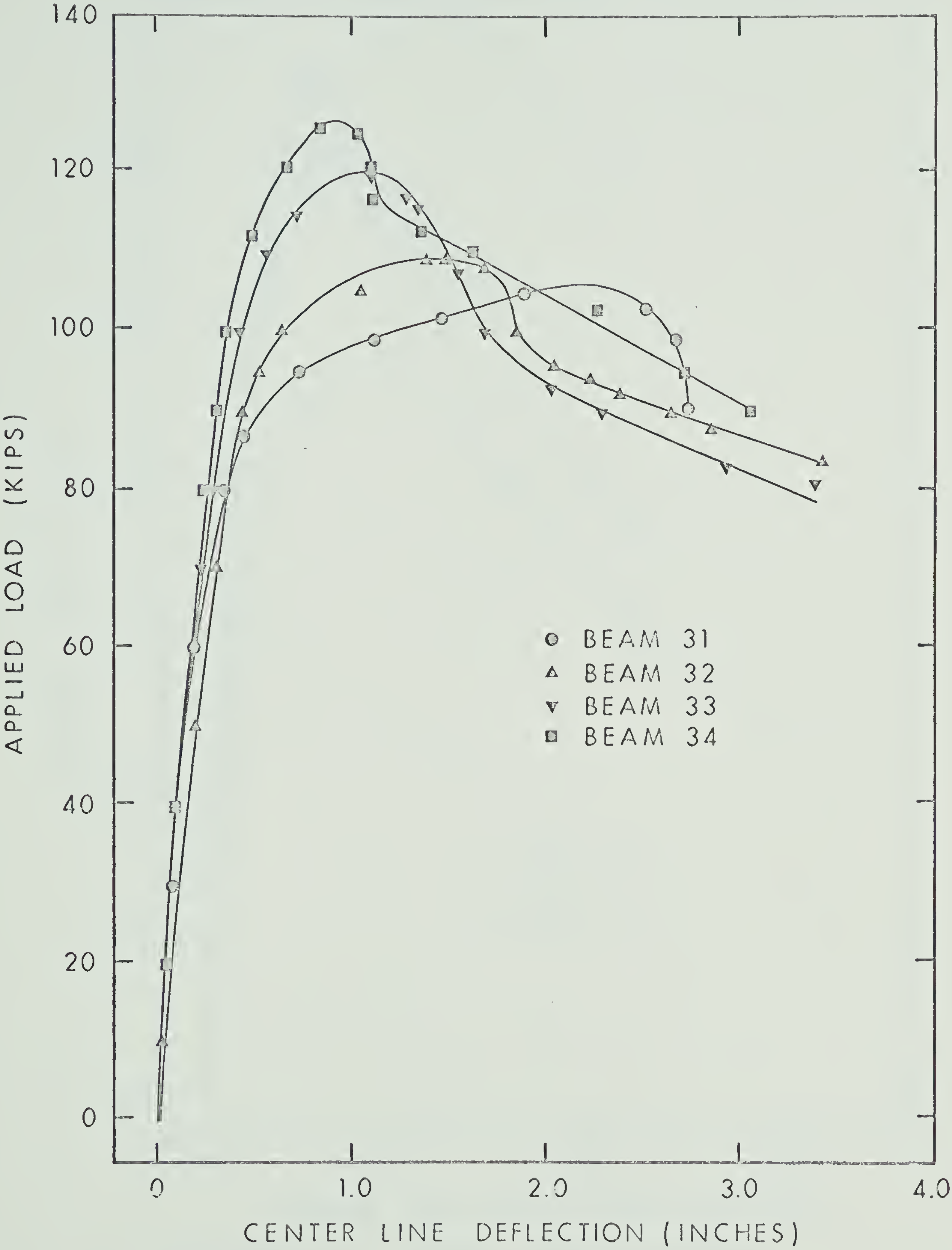

FIGURE 3.2 LOAD-DEFLECTION RELATIONSHIPS

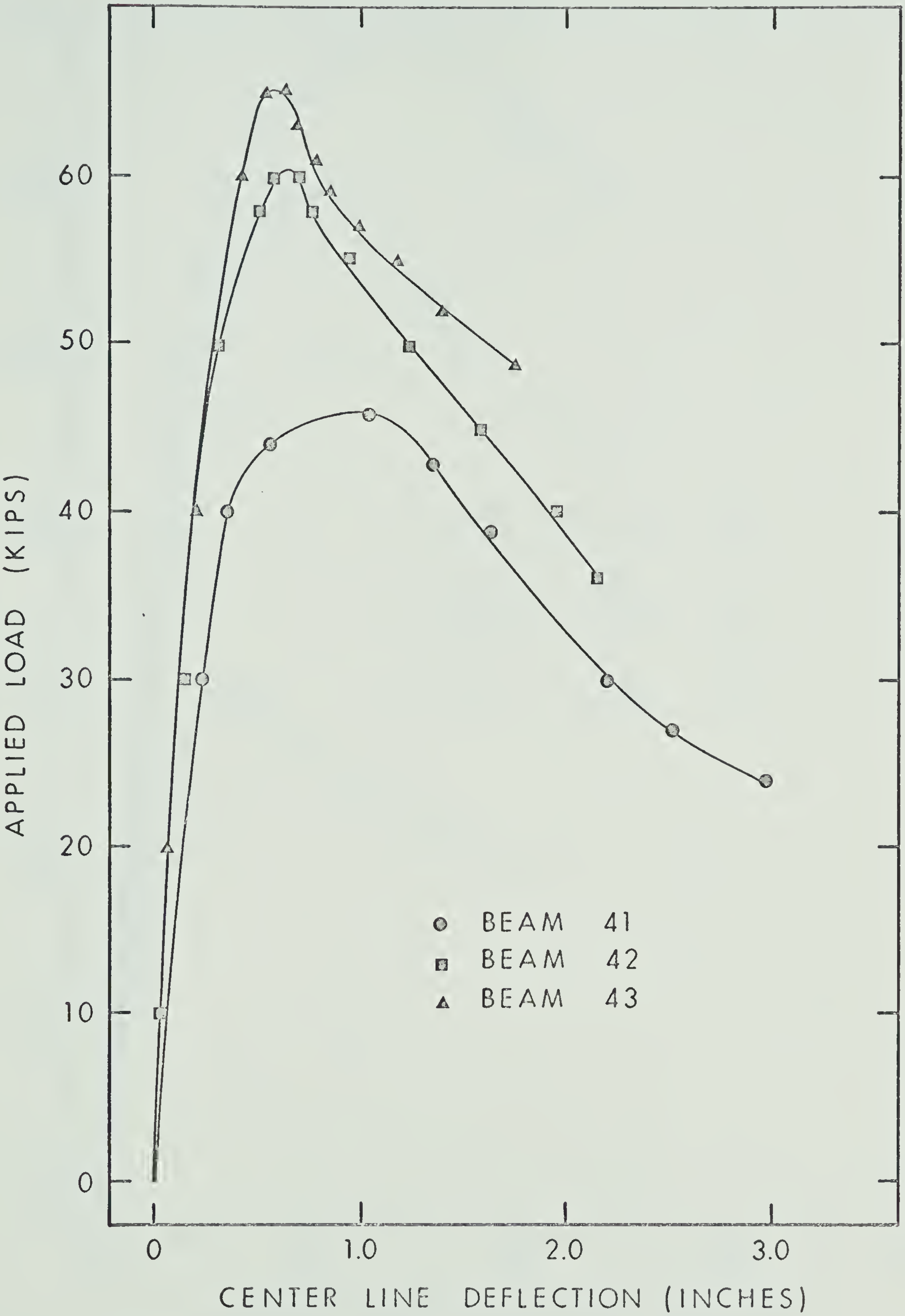

FIGURE 3.3 LOAD - DEFLECTION RELATIONSHIPS

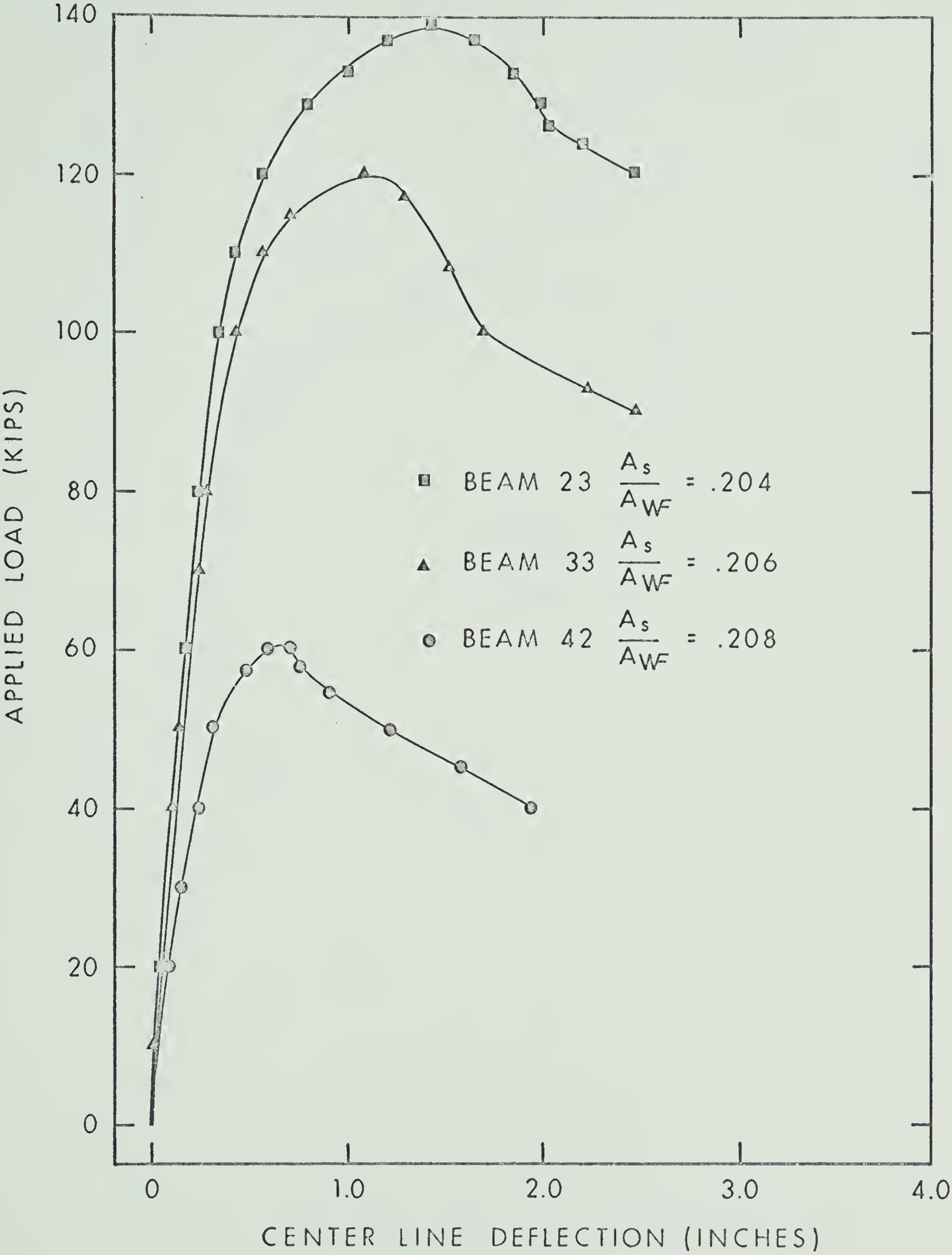

FIGURE 3.4 LOAD - DEFLECTION RELATIONSHIPS

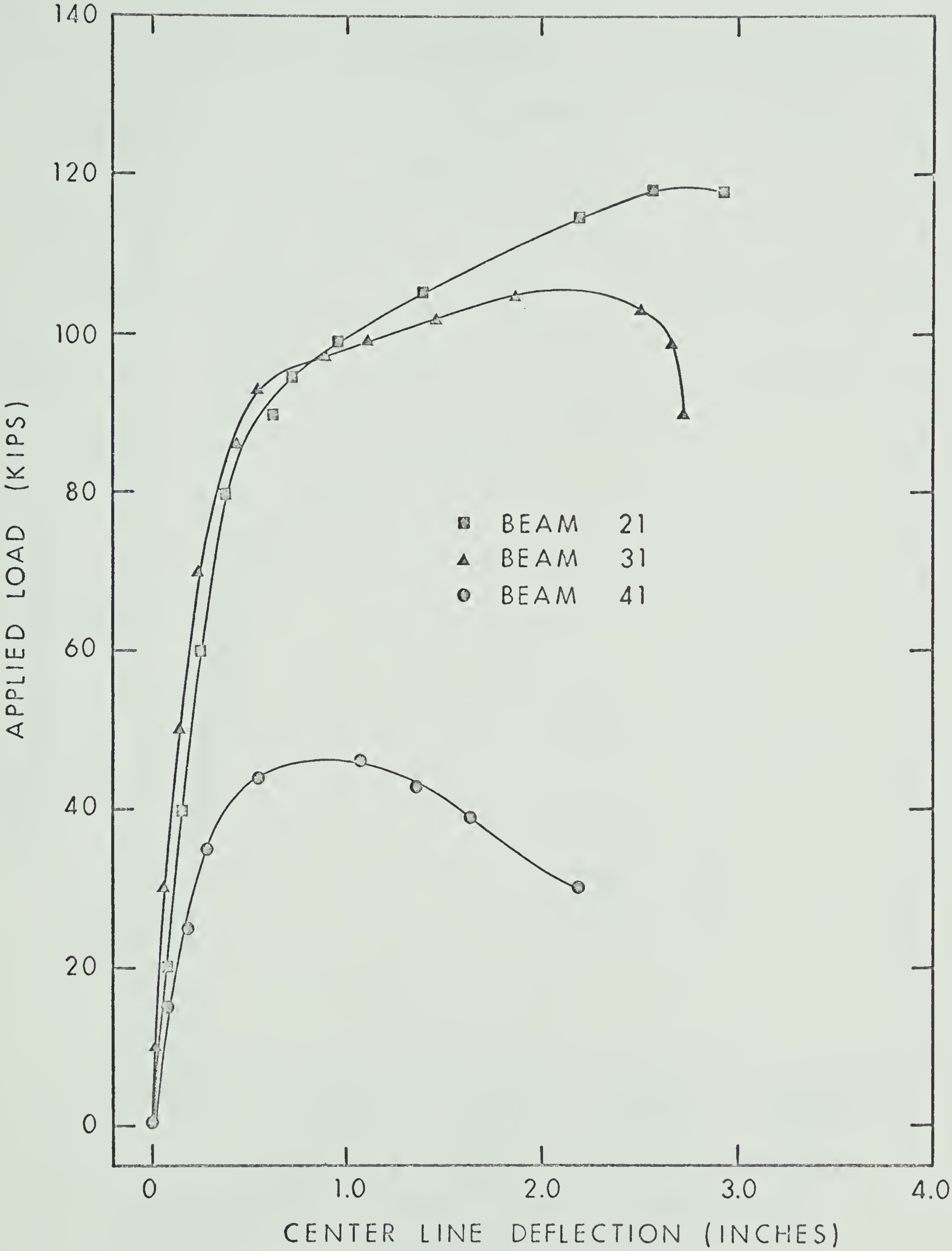

FIGURE 3.5 LOAD-DEFLECTION RELATIONSHIPS

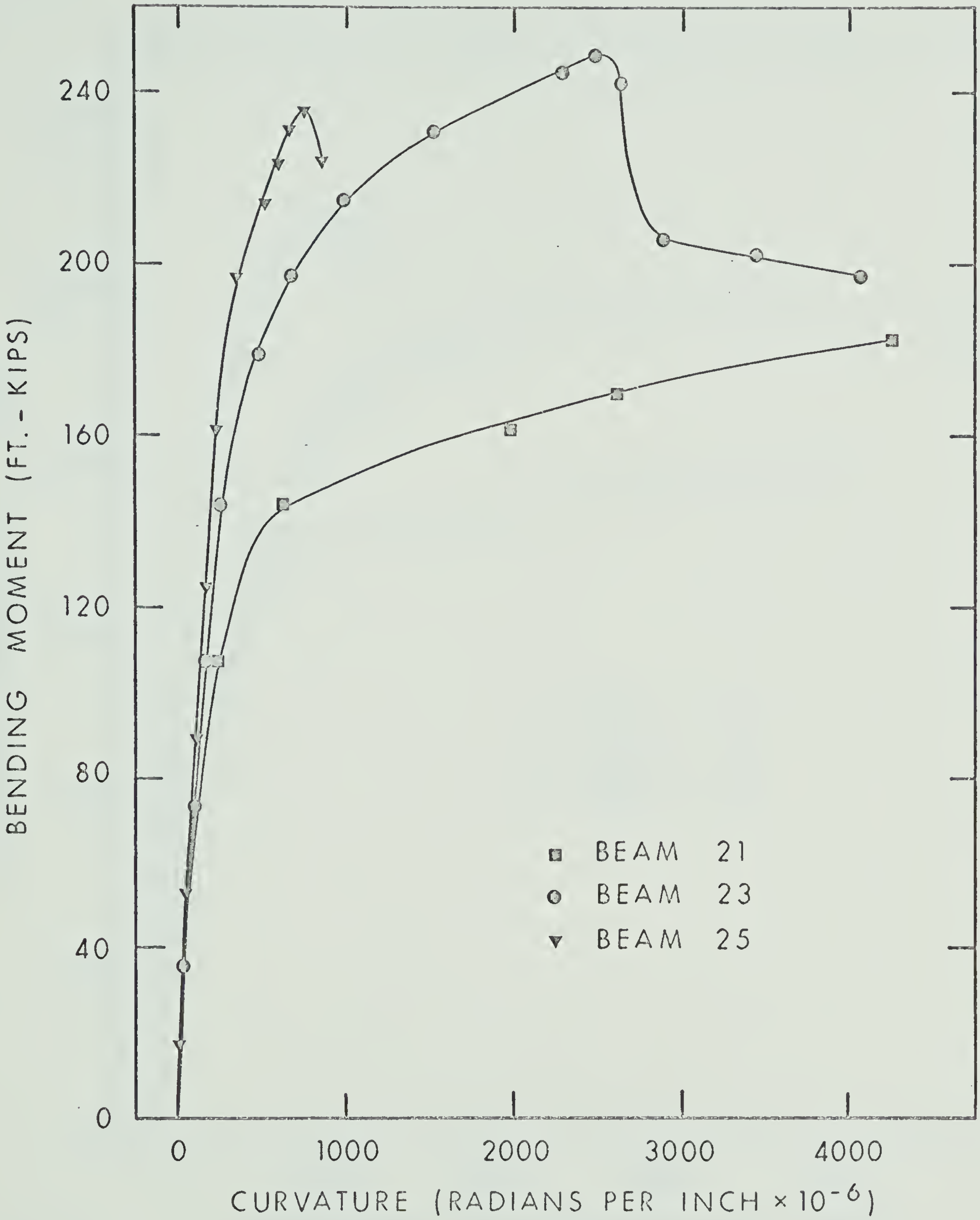

FIGURE 3.6 MOMENT - CURVATURE RELATIONSHIPS

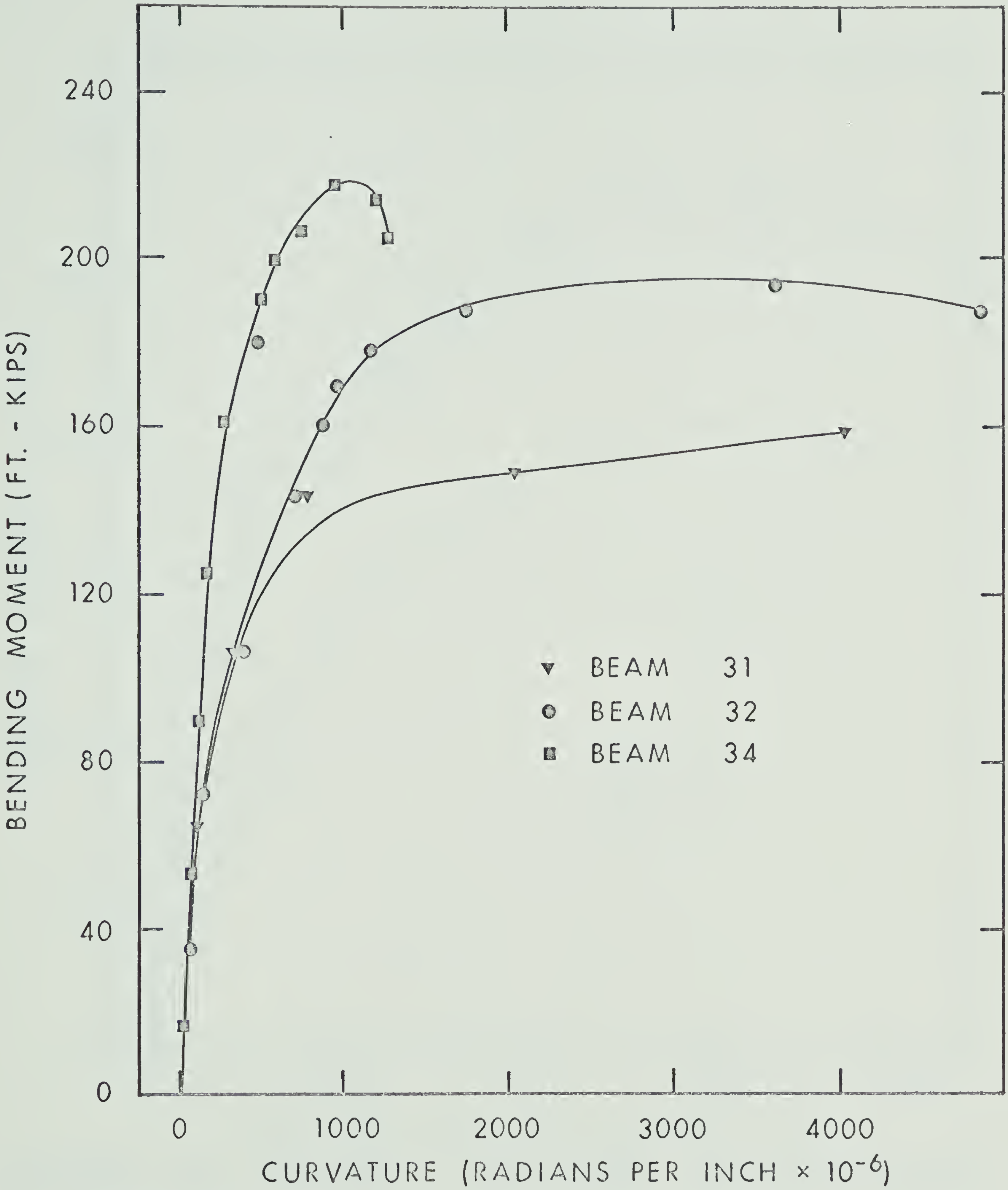

FIGURE 3.7 MOMENT-CURVATURE RELATIONSHIPS

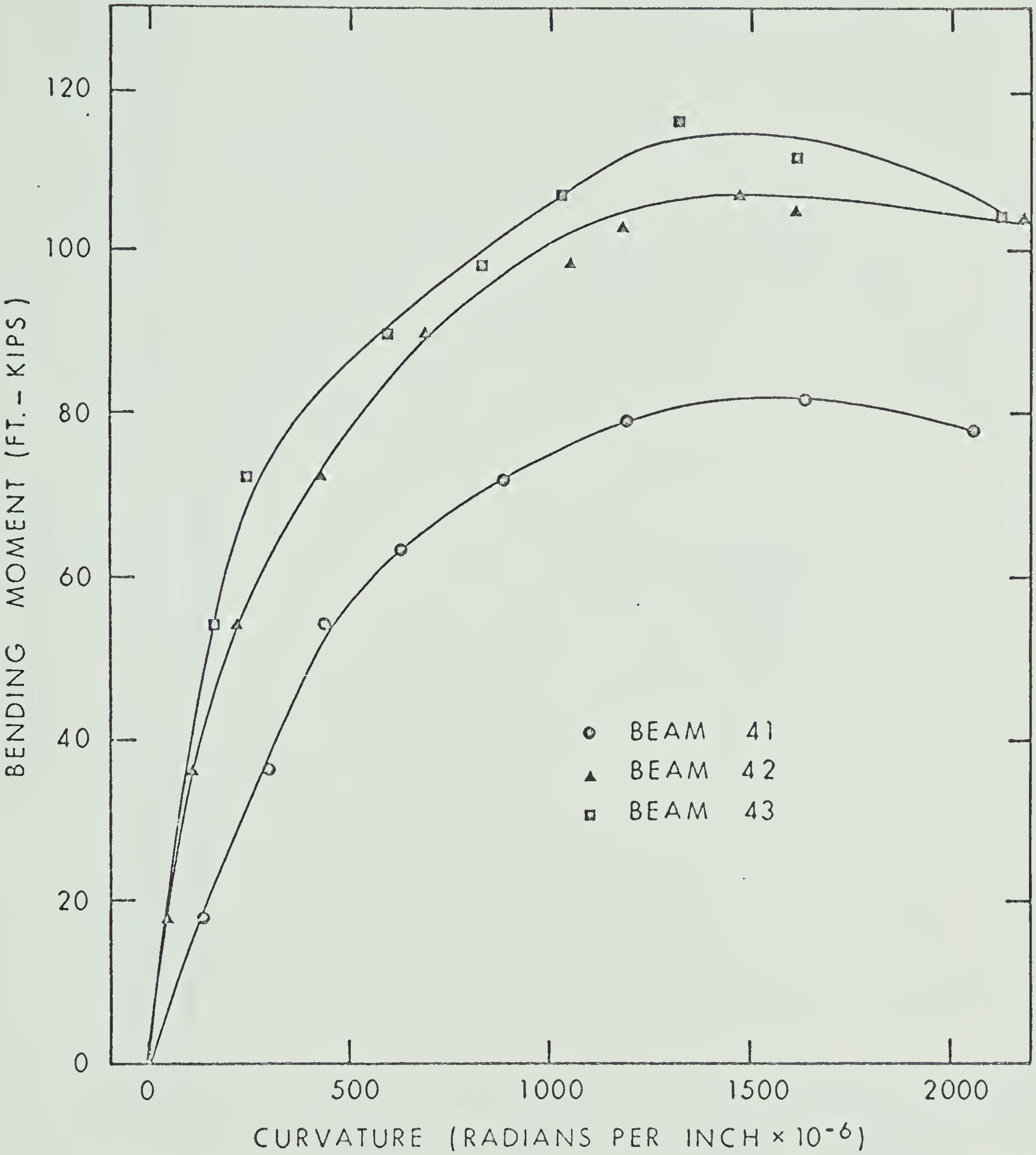

FIGURE 3.8 MOMENT - CURVATURE RELATIONSHIPS

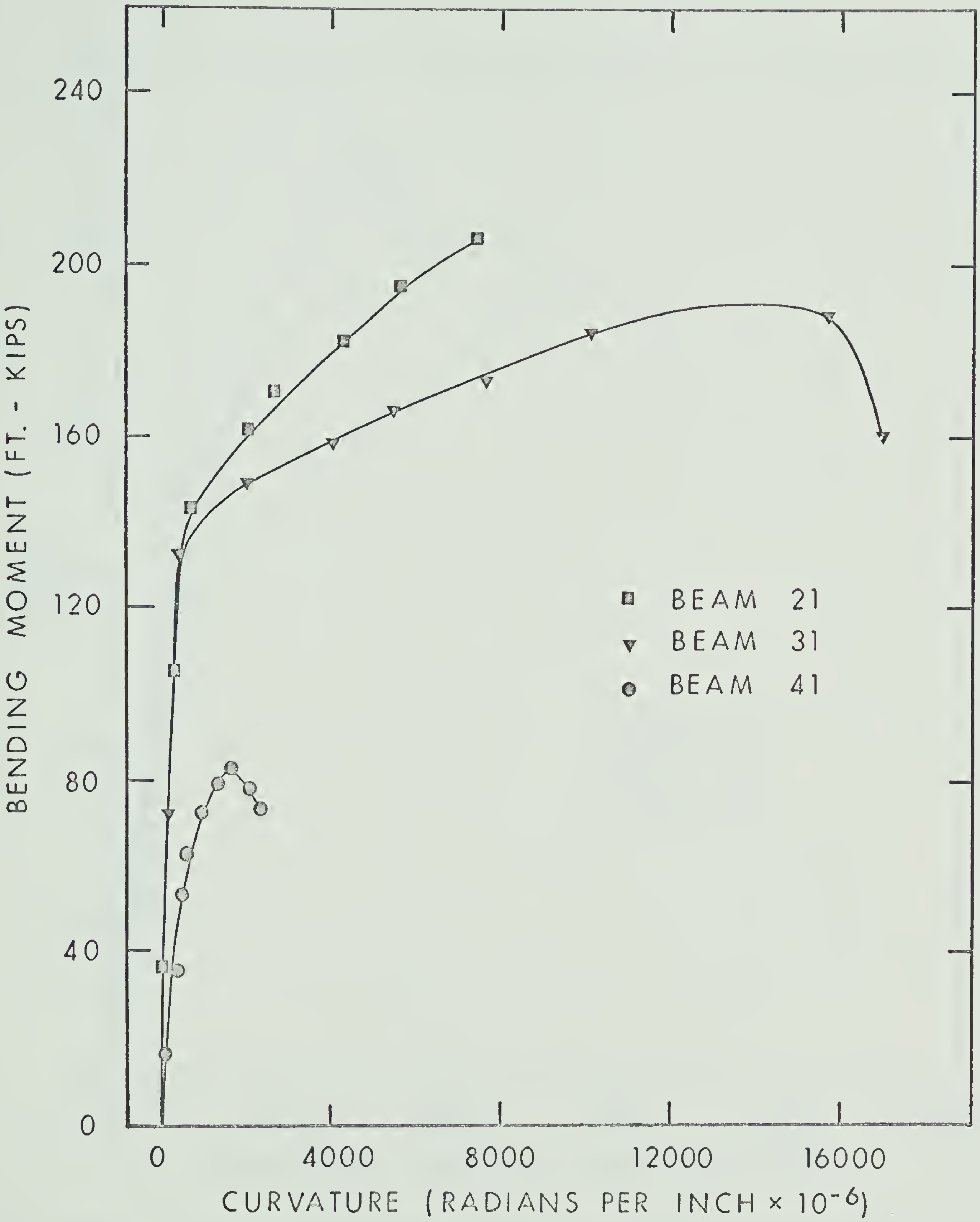

FIGURE 3.9 MOMENT - CURVATURE RELATIONSHIPS

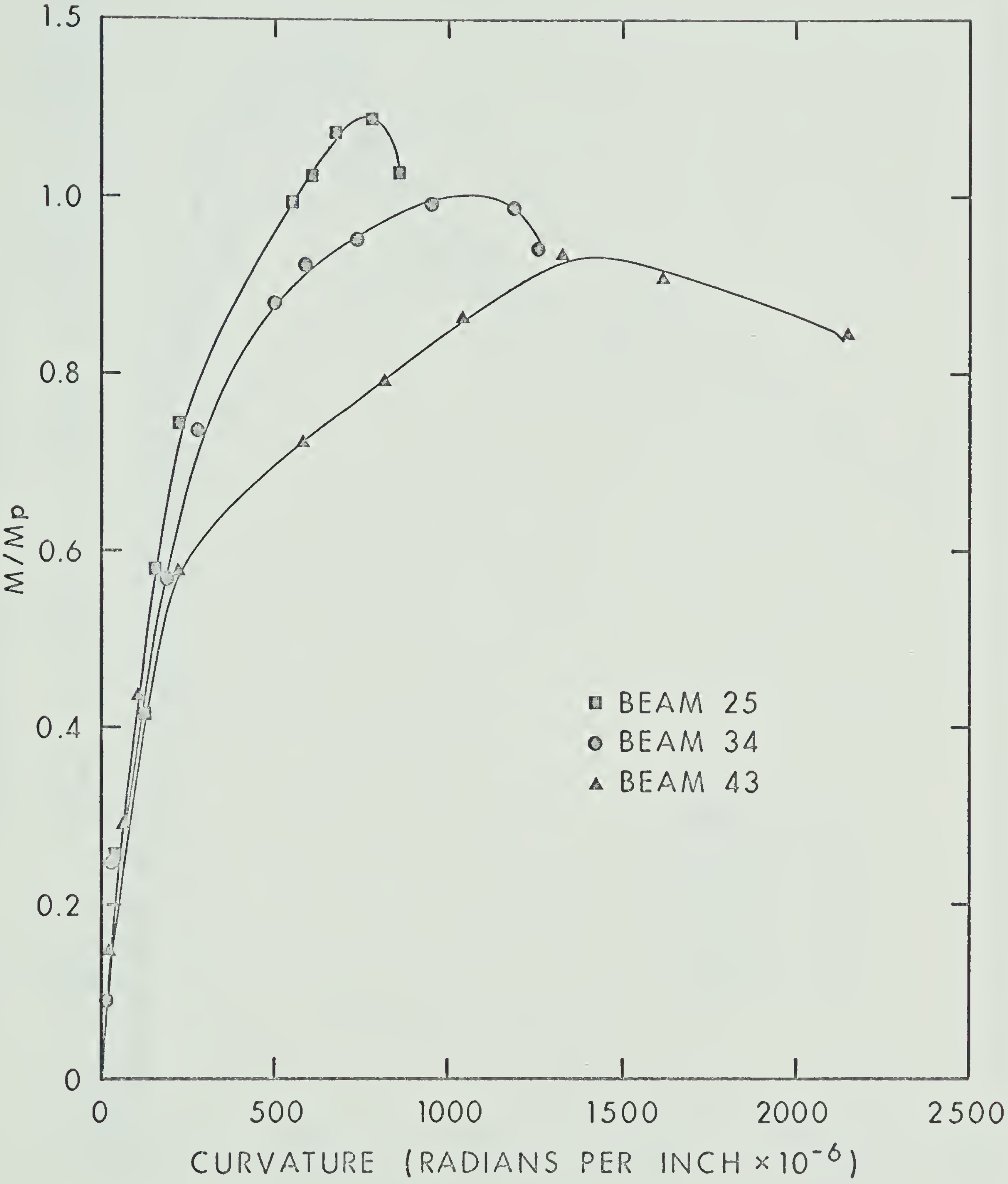

FIGURE 3.10 MOMENT - CURVATURE RELATIONSHIPS

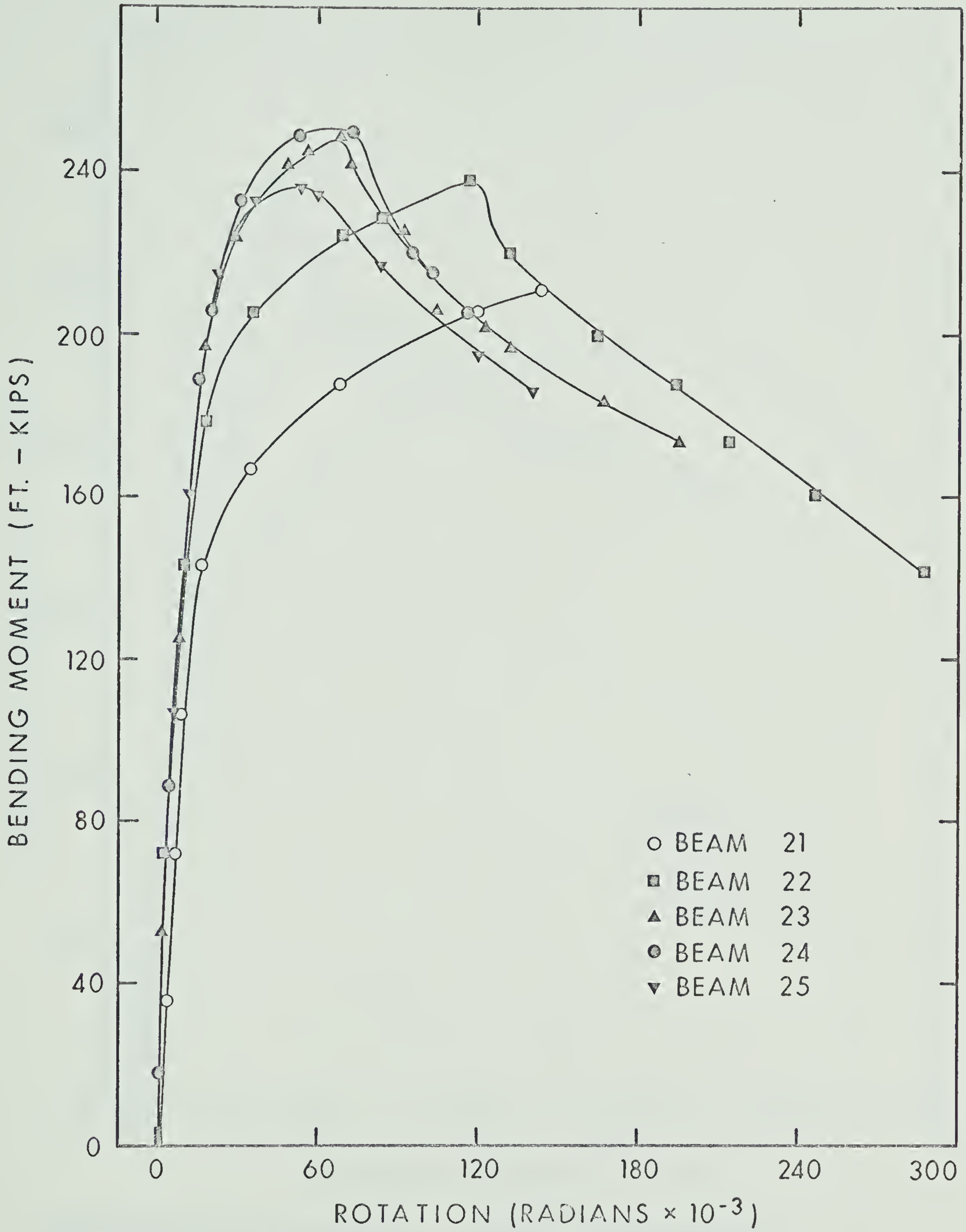

FIGURE 3.11 MOMENT — TOTAL ROTATION RELATIONSHIPS

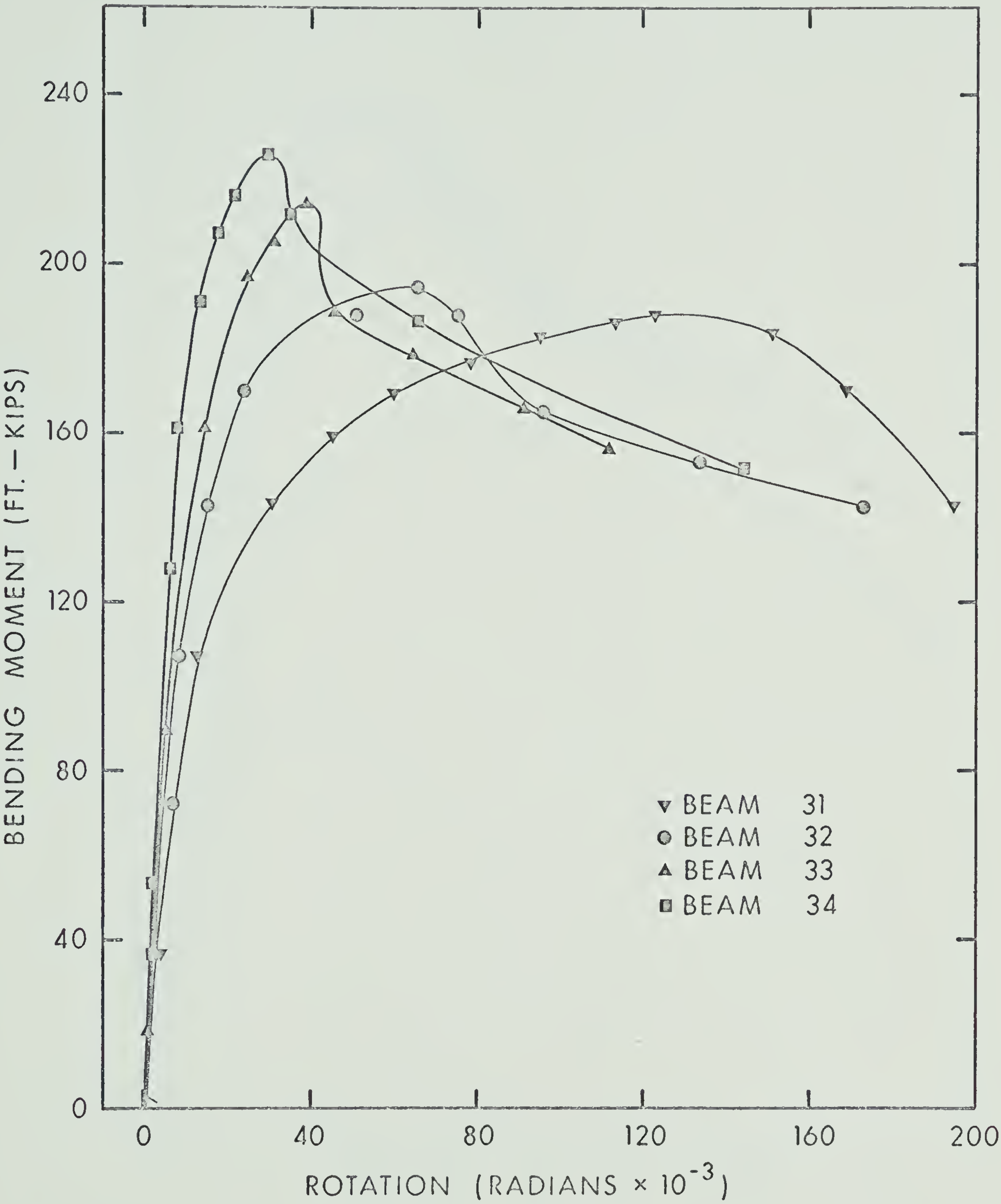

FIGURE 3.12 MOMENT — TOTAL ROTATION RELATIONSHIPS

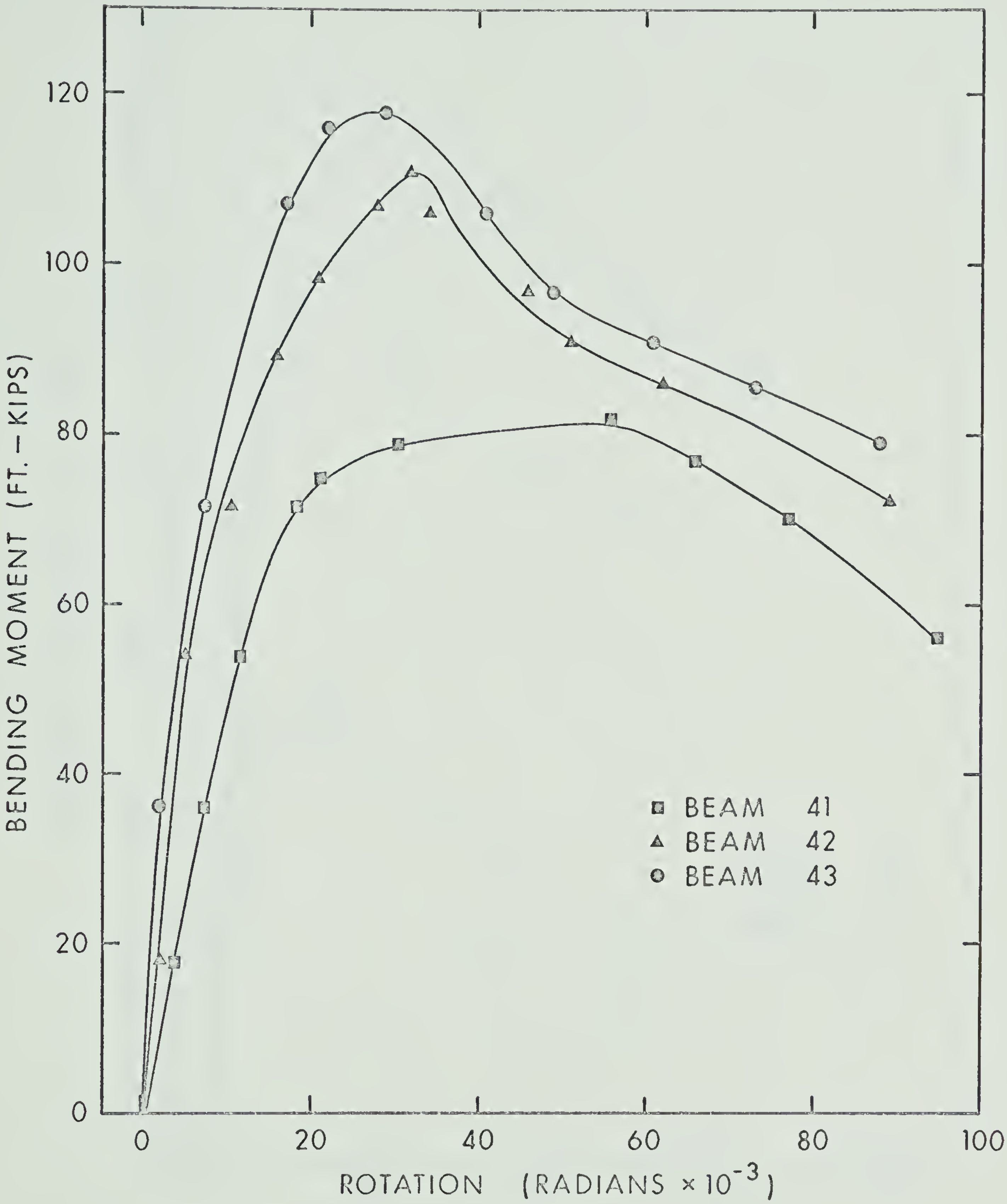

FIGURE 3.13 MOMENT — TOTAL ROTATION RELATIONSHIPS

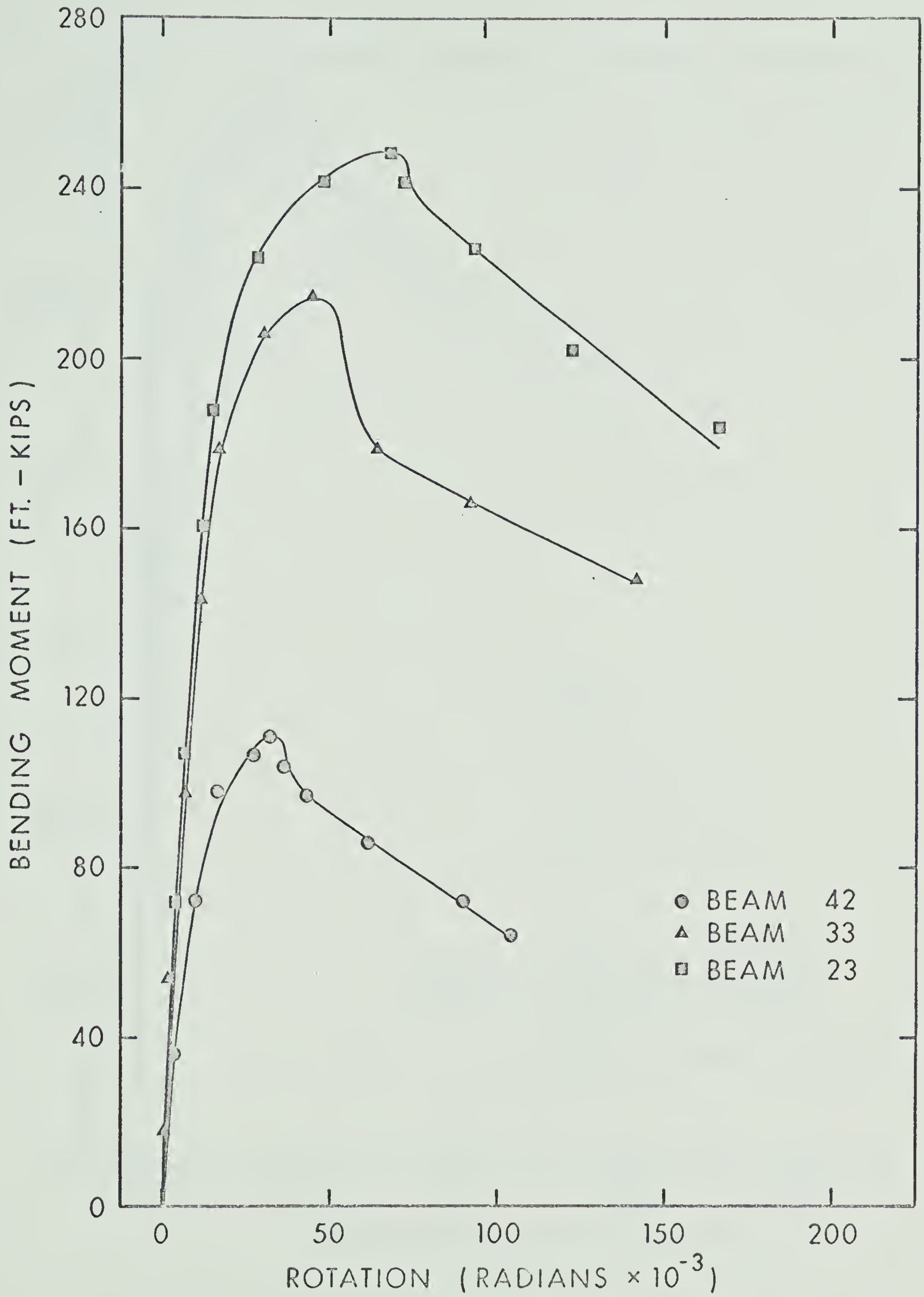

FIGURE 3.14 MOMENT - TOTAL ROTATION RELATIONSHIPS

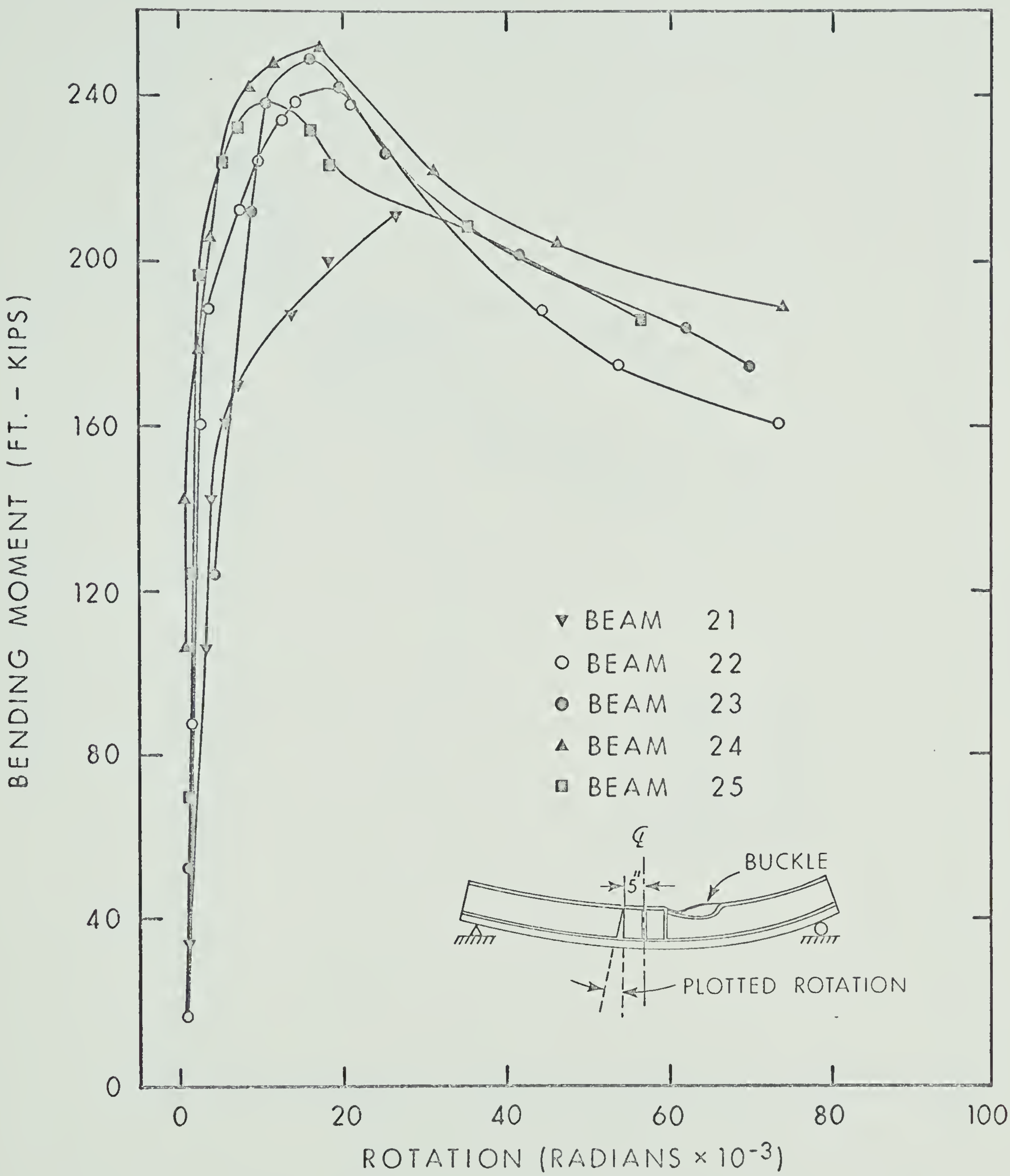

FIGURE 3.15 MOMENT-ROTATION RELATIONSHIPS

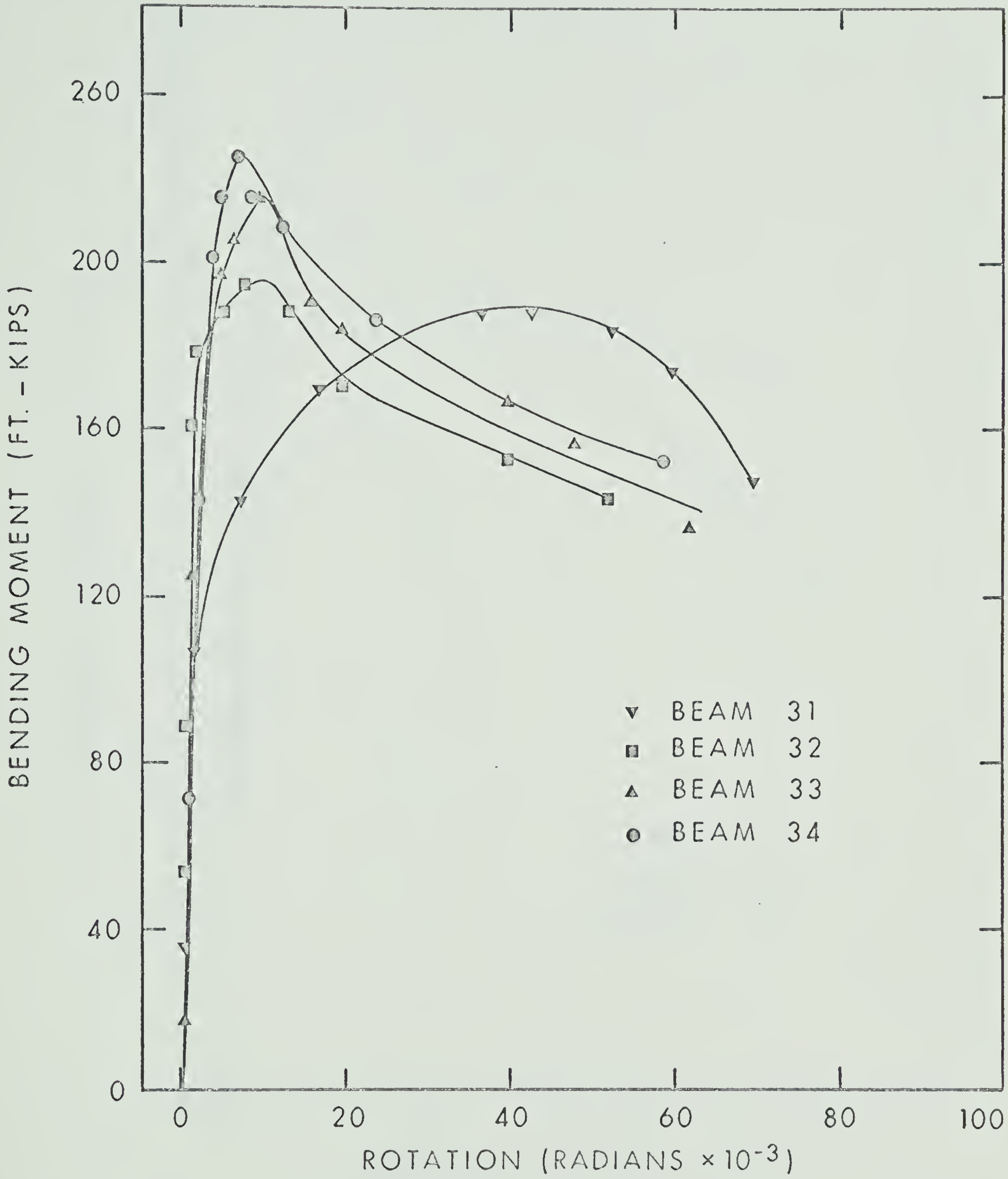

FIGURE 3.16 MOMENT-ROTATION RELATIONSHIPS

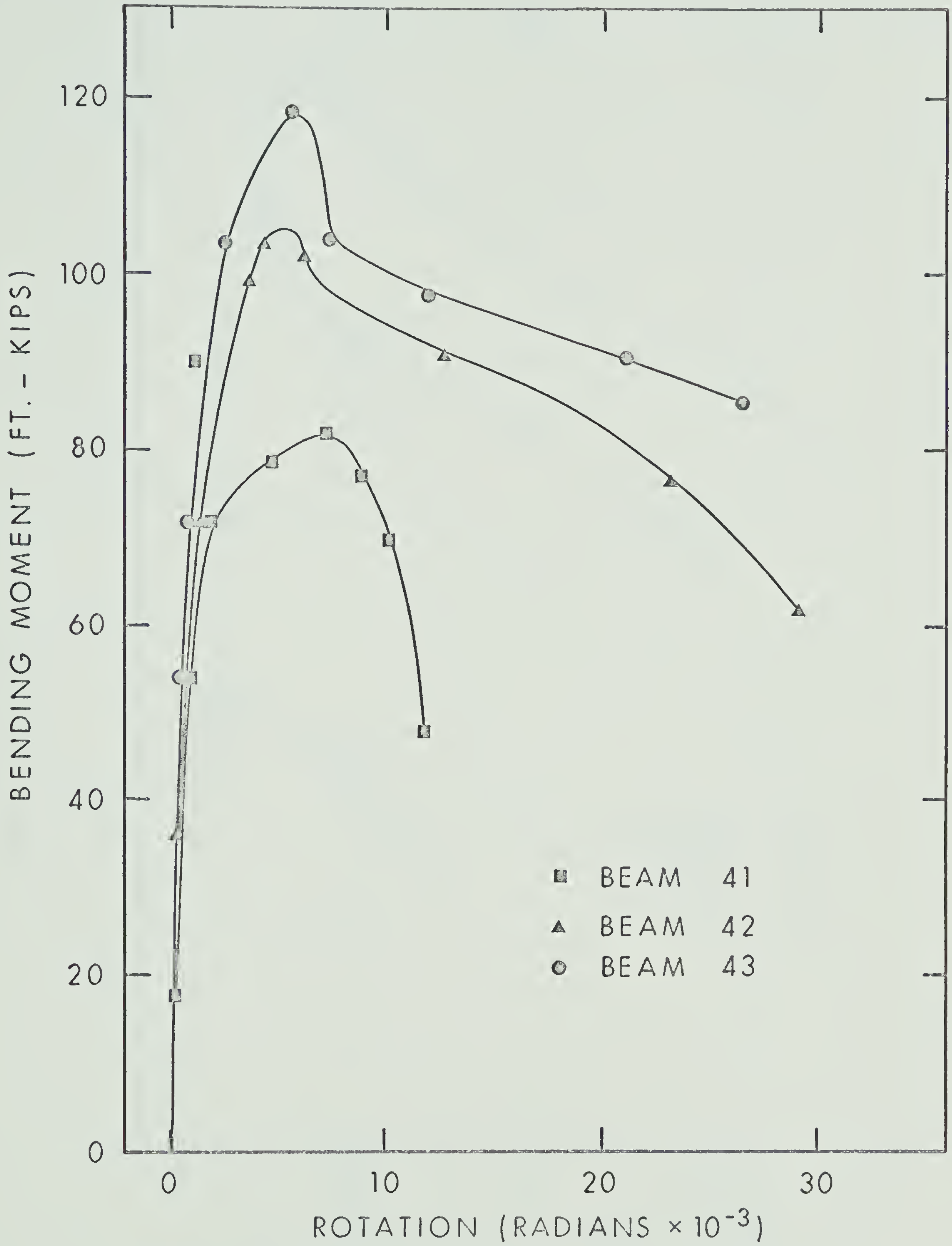

FIGURE 3.17 MOMENT-ROTATION RELATIONSHIPS

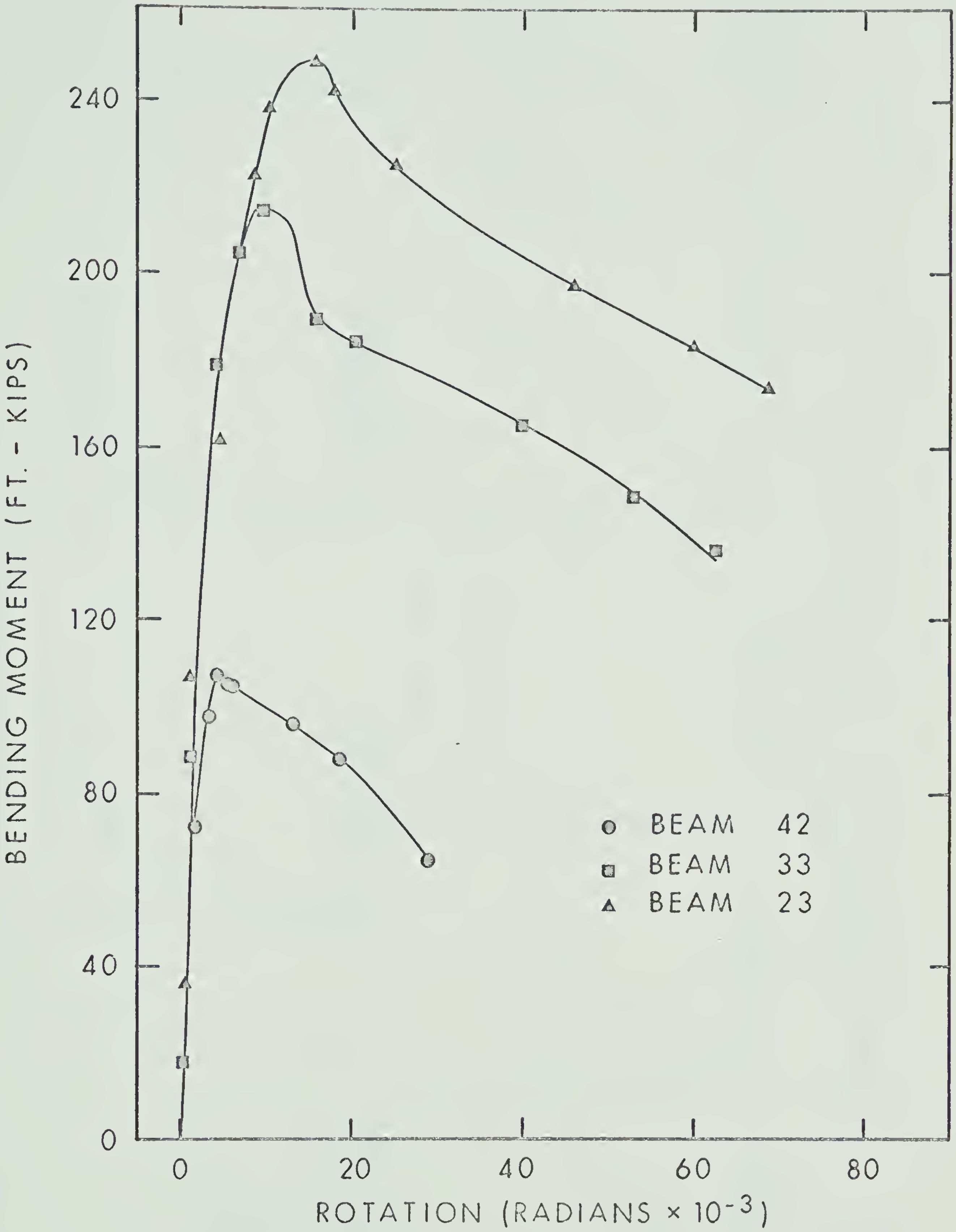

FIGURE 3.18 MOMENT– ROTATION RELATIONSHIPS

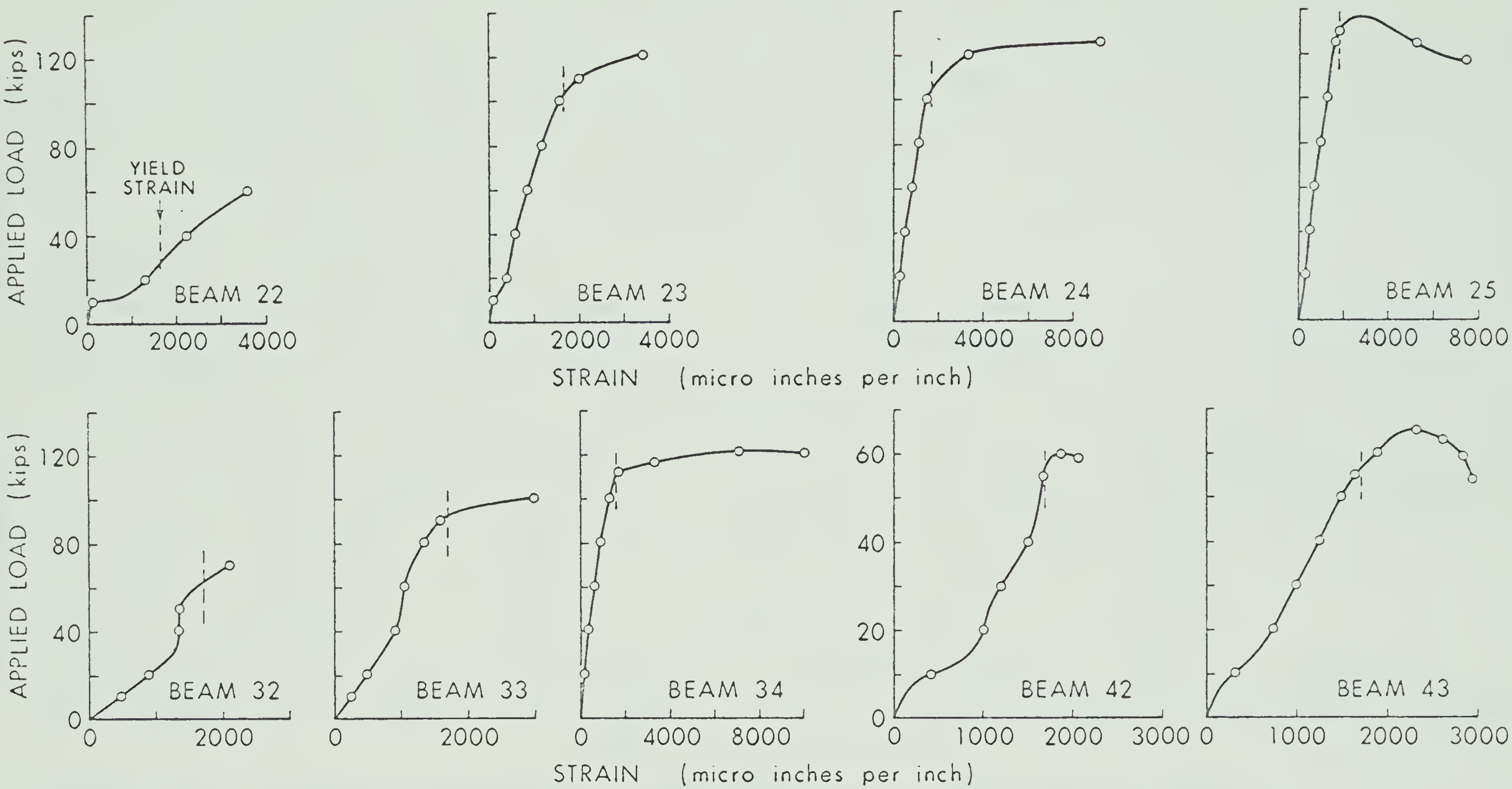

FIGURE 3·19 MIDSPAN LONGITUDINAL REINFORCEMENT STRAINS ON "A" BARS

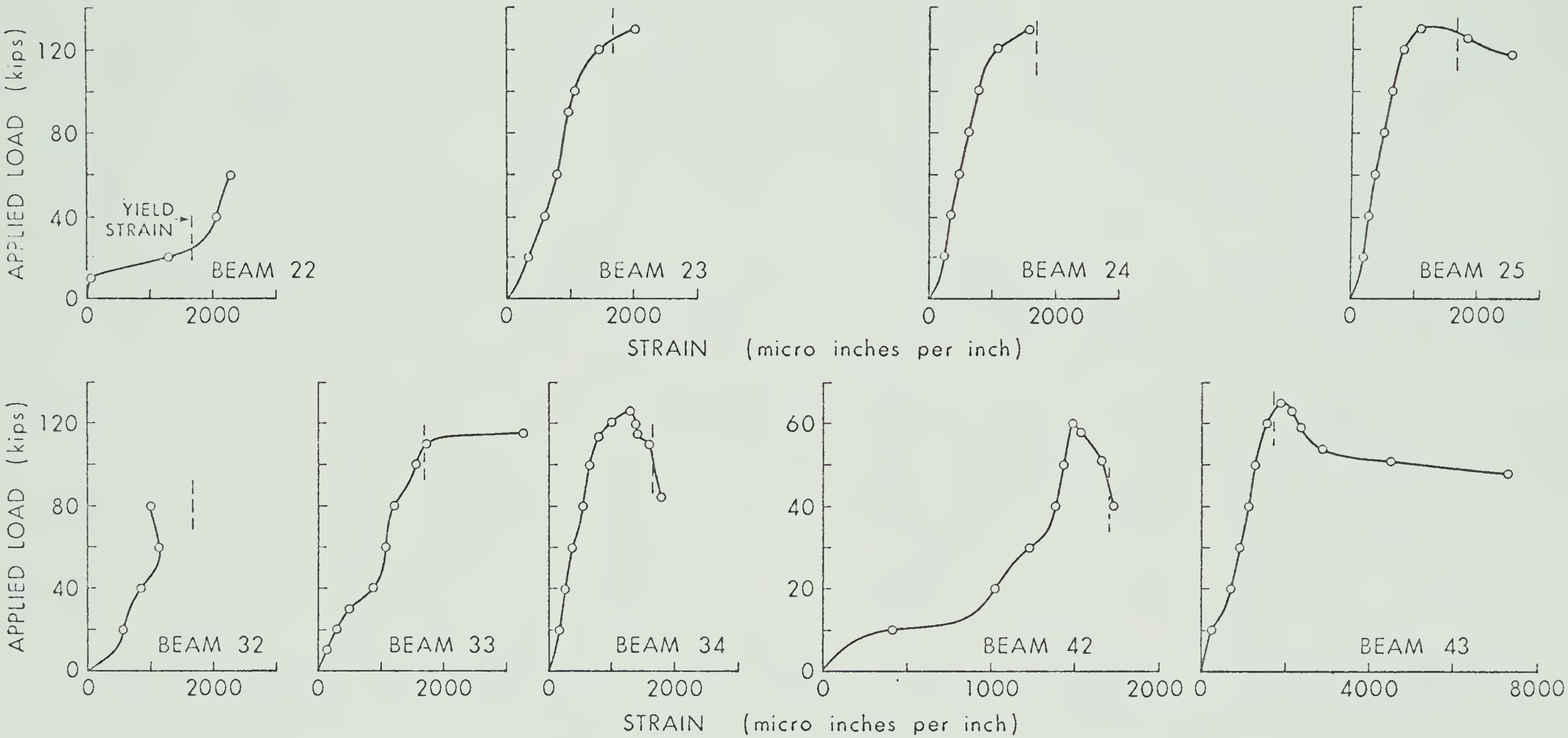

FIGURE 3·20 MIDSPAN LONGITUDINAL REINFORCEMENT STRAINS ON "B" BARS

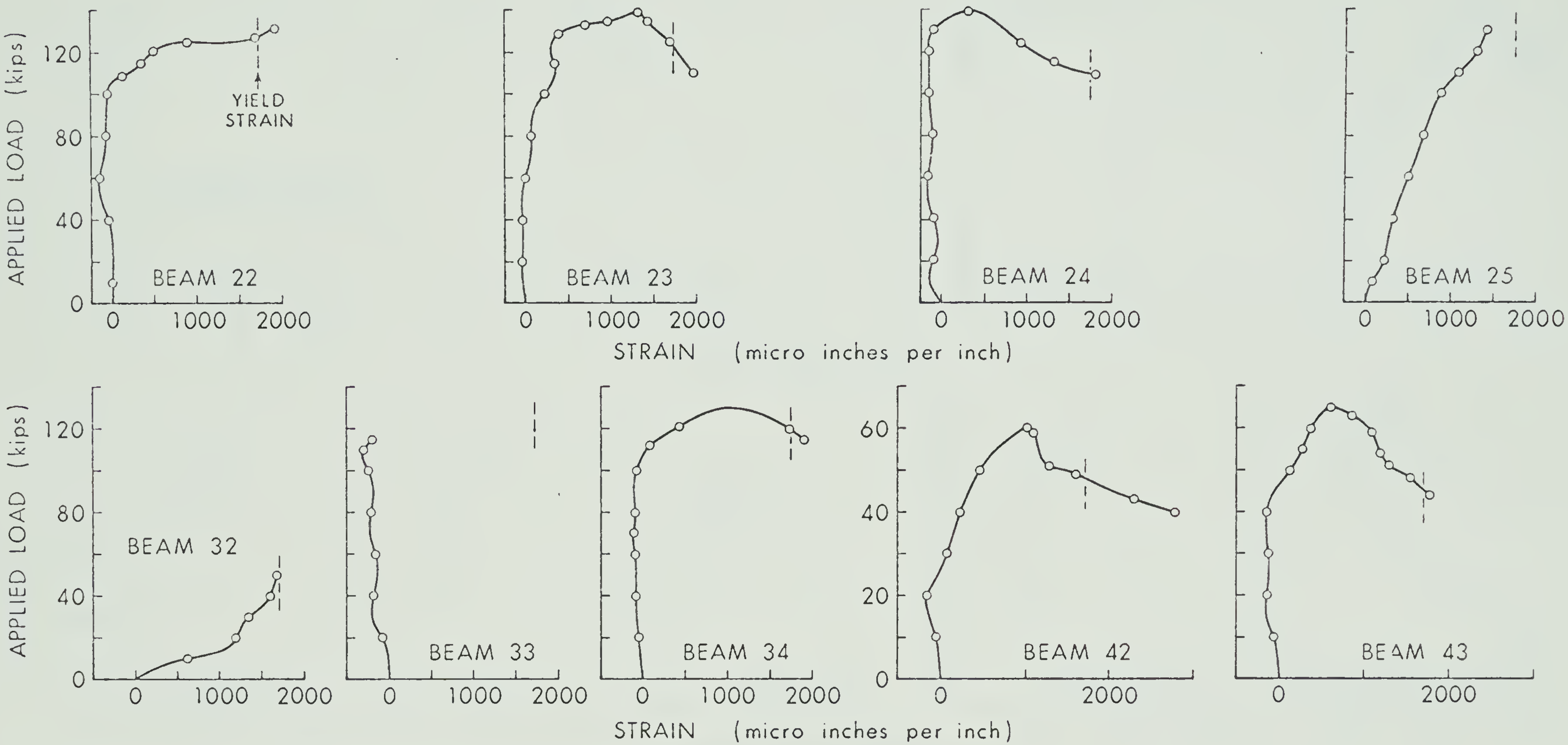

FIGURE 3·21 MIDSPAN TRANSVERSE REINFORCEMENT STRAINS

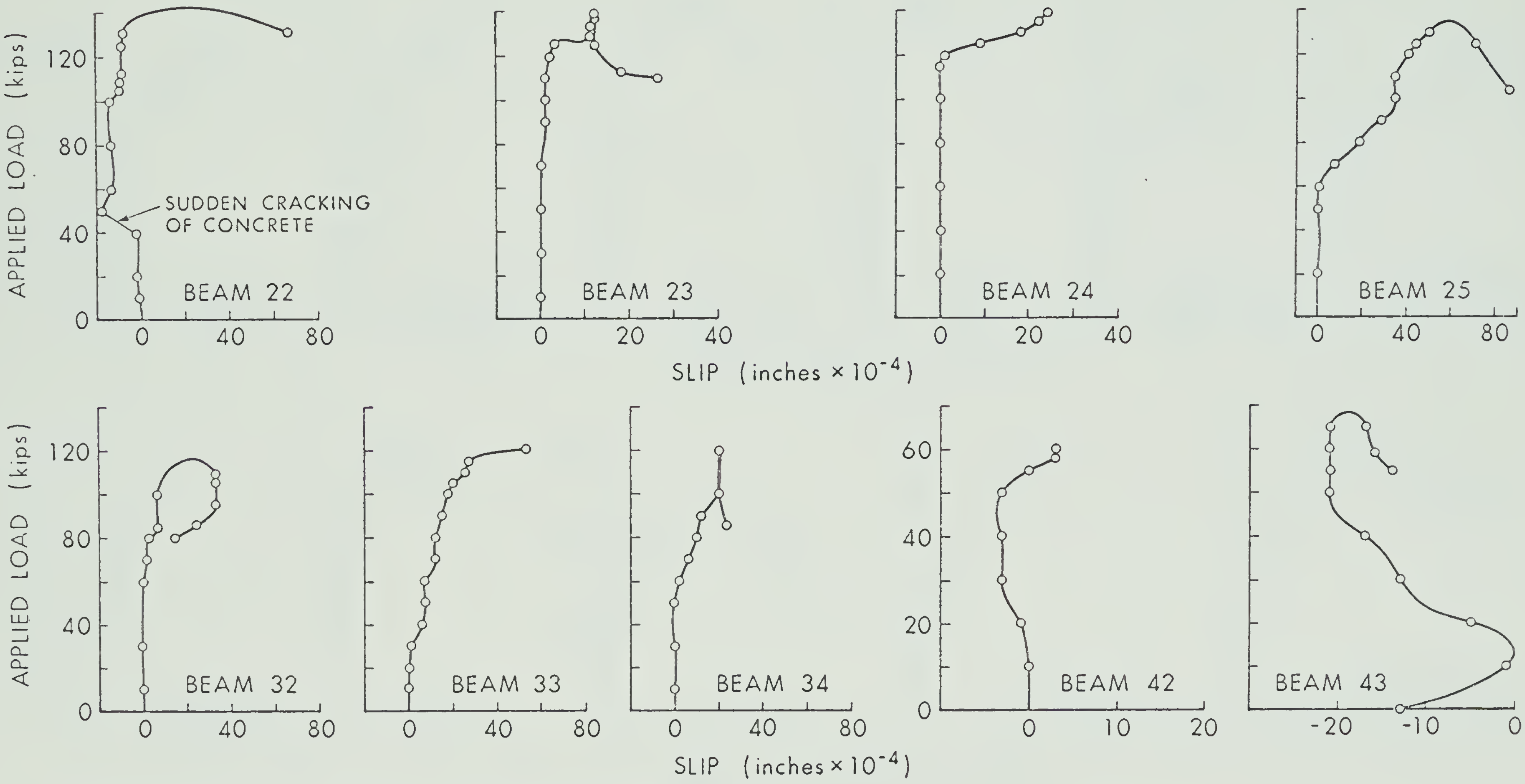

FIGURE 3·22 LOAD - SLIP RELATIONSHIPS

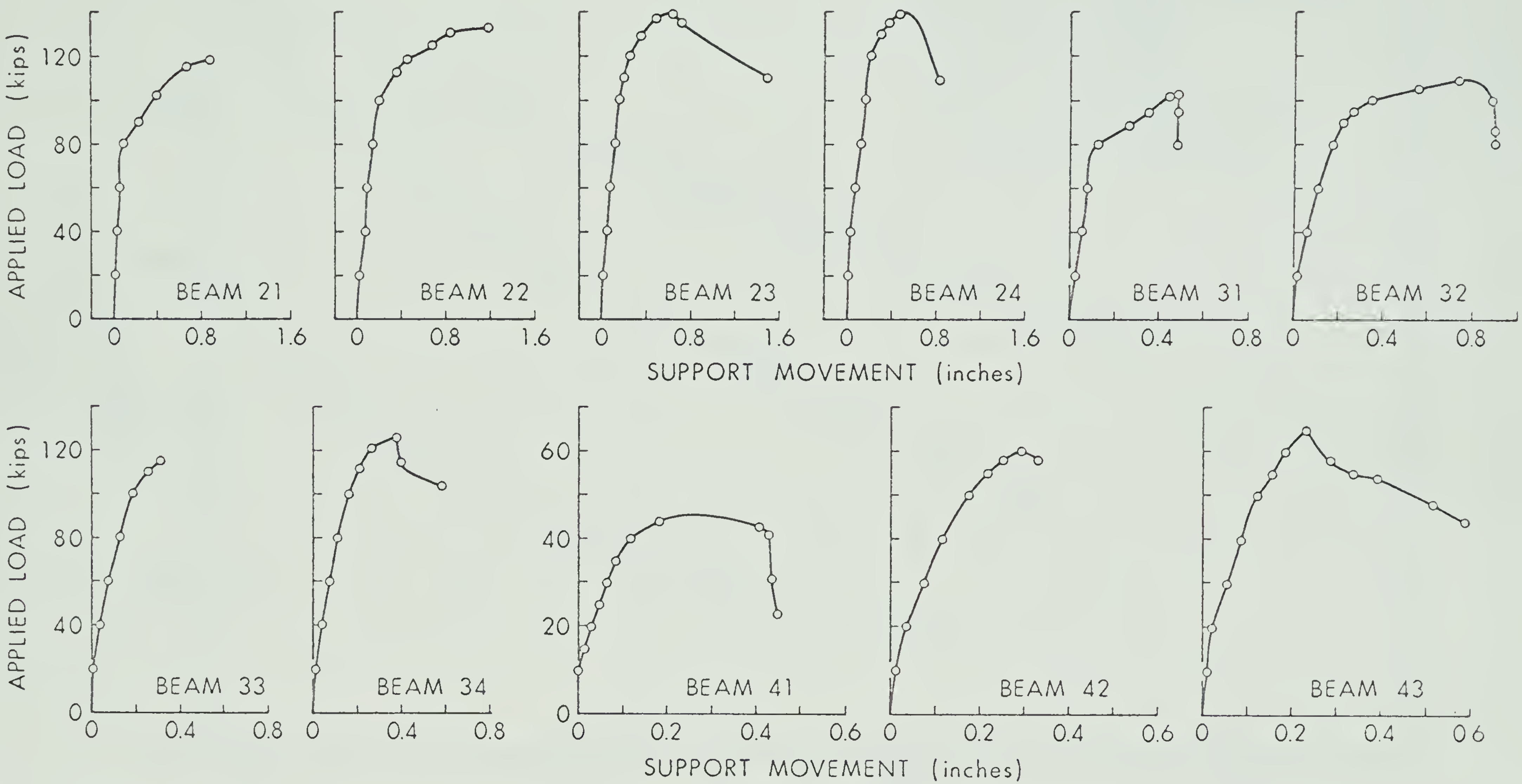

FIGURE 3·23 LOAD - SUPPORT MOVEMENT RELATIONSHIPS

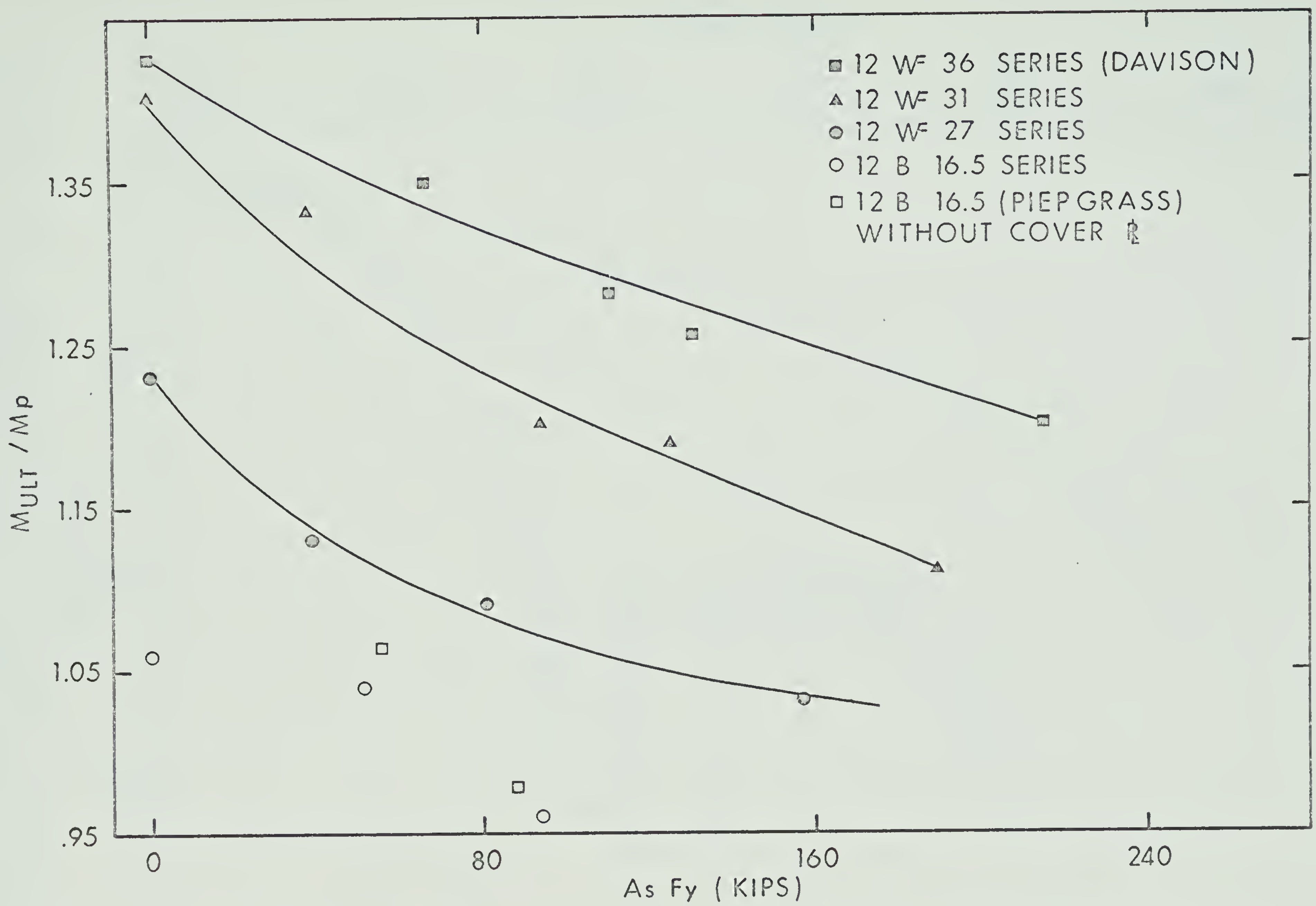

FIGURE 3.24 VARIATION IN M_{ULT} / M_p WITH INCREASING SLAB REINFORCEMENT

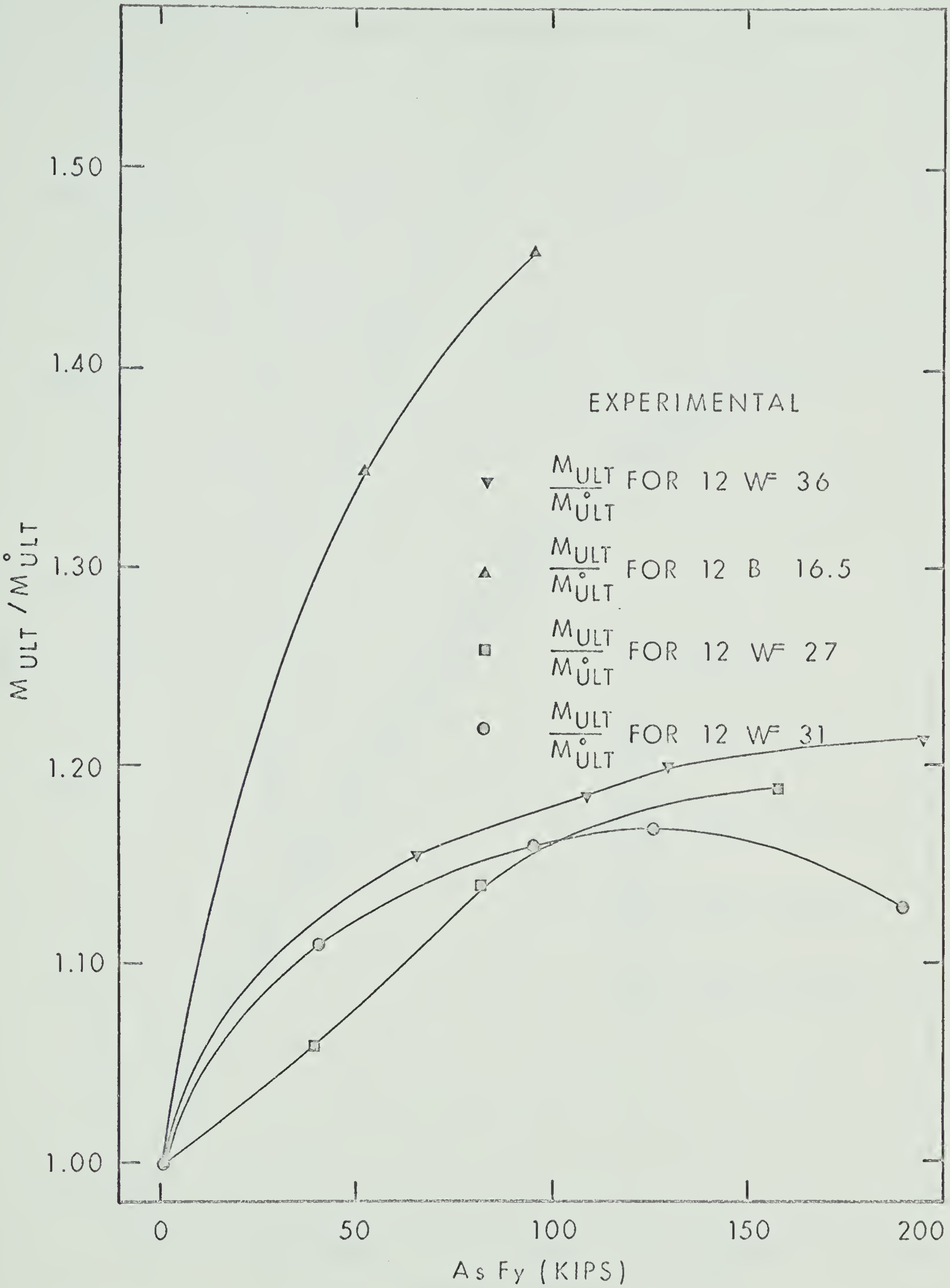

FIGURE 3.25 RELATIONSHIP BETWEEN MOMENT RATIO M_{ULT}/M°_{ULT} AND YIELD FORCE IN SLAB REINFORCEMENT AsFy.

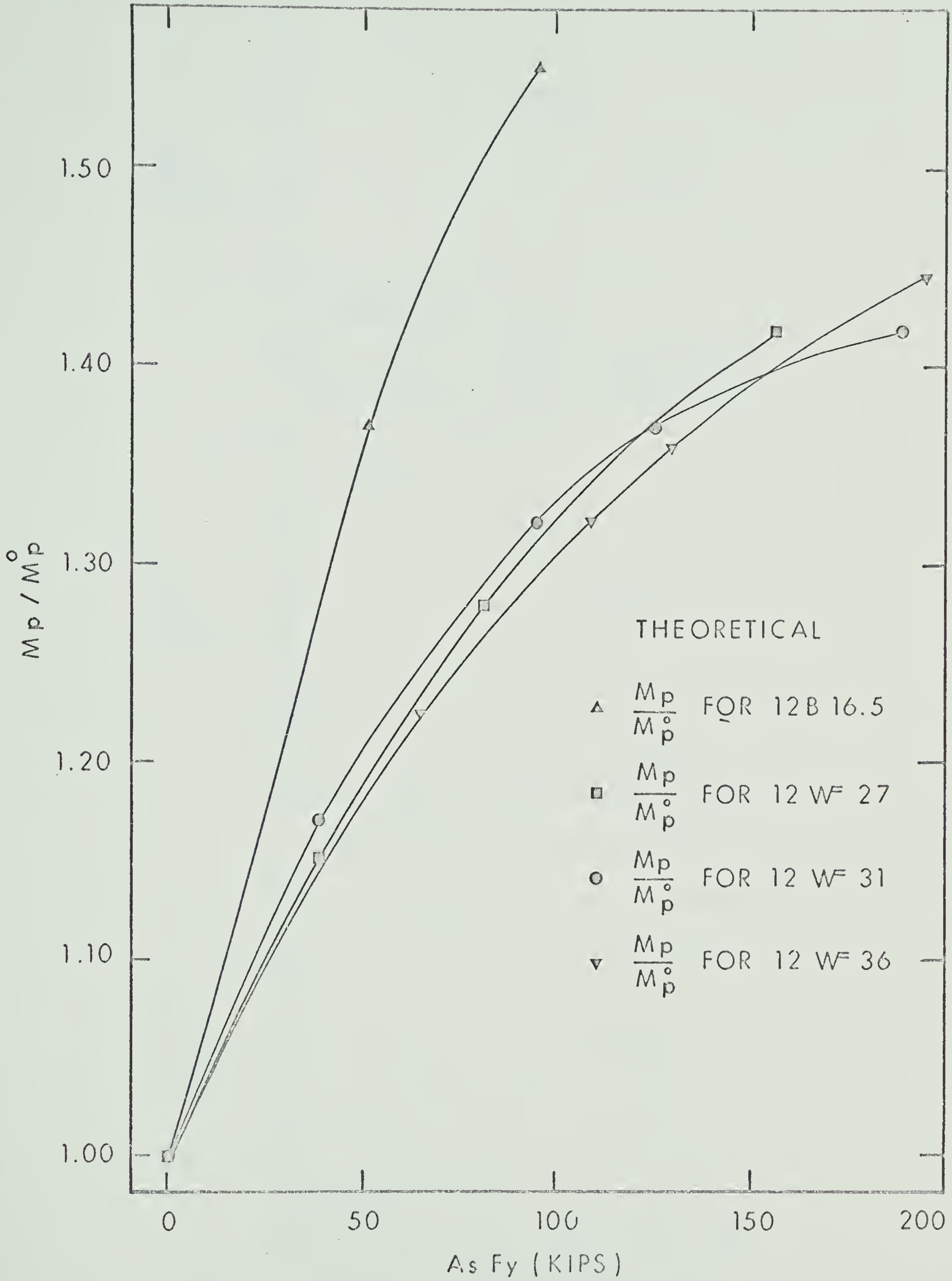

FIGURE 3.26 RELATIONSHIP BETWEEN MOMENT RATIO M_p/M_p° AND YIELD FORCE REINFORCEMENT $A_s F_y$ IN SLAB.

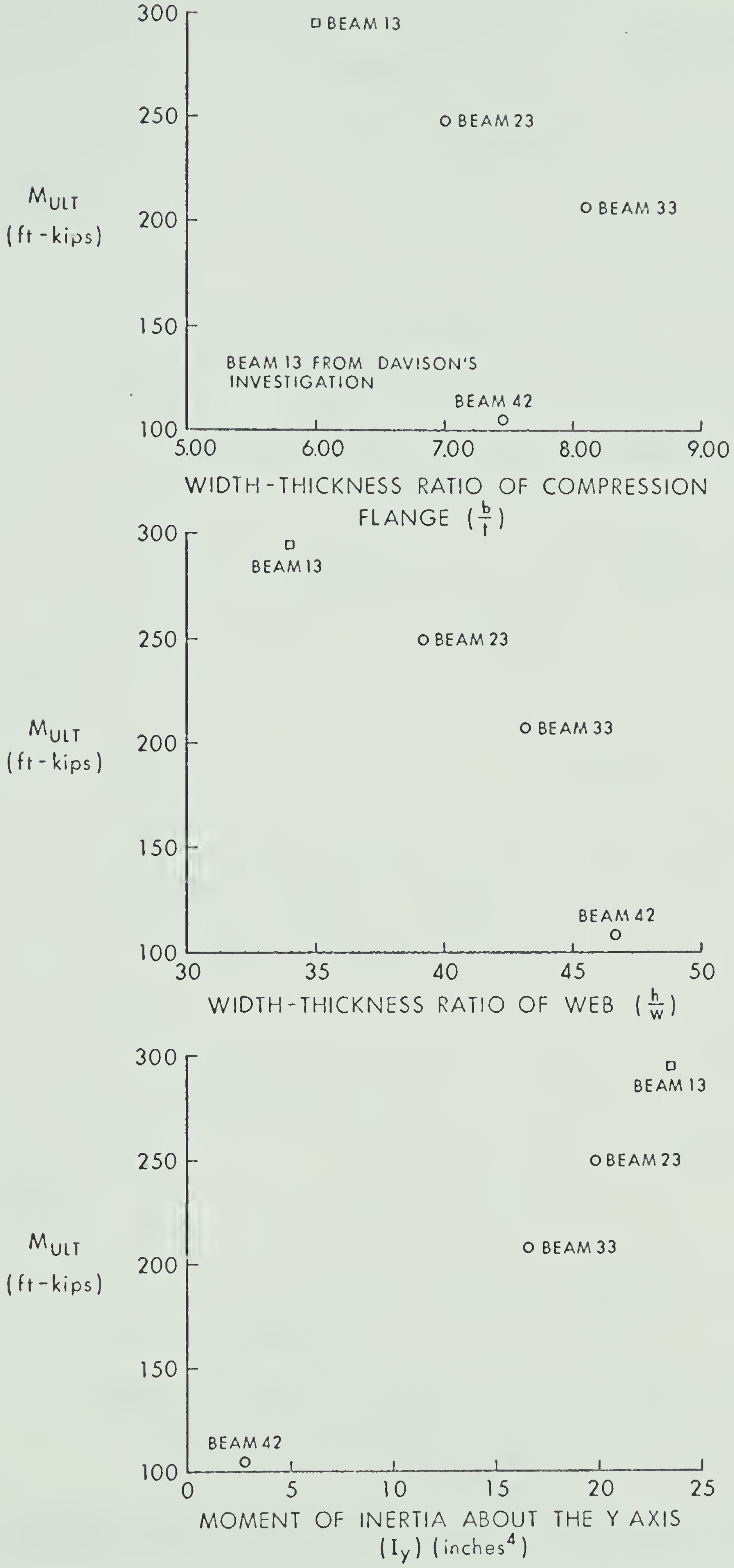

FIGURE 3·27 RELATIONSHIPS BETWEEN ULTIMATE MOMENT AND STEEL SECTION PARAMETERS

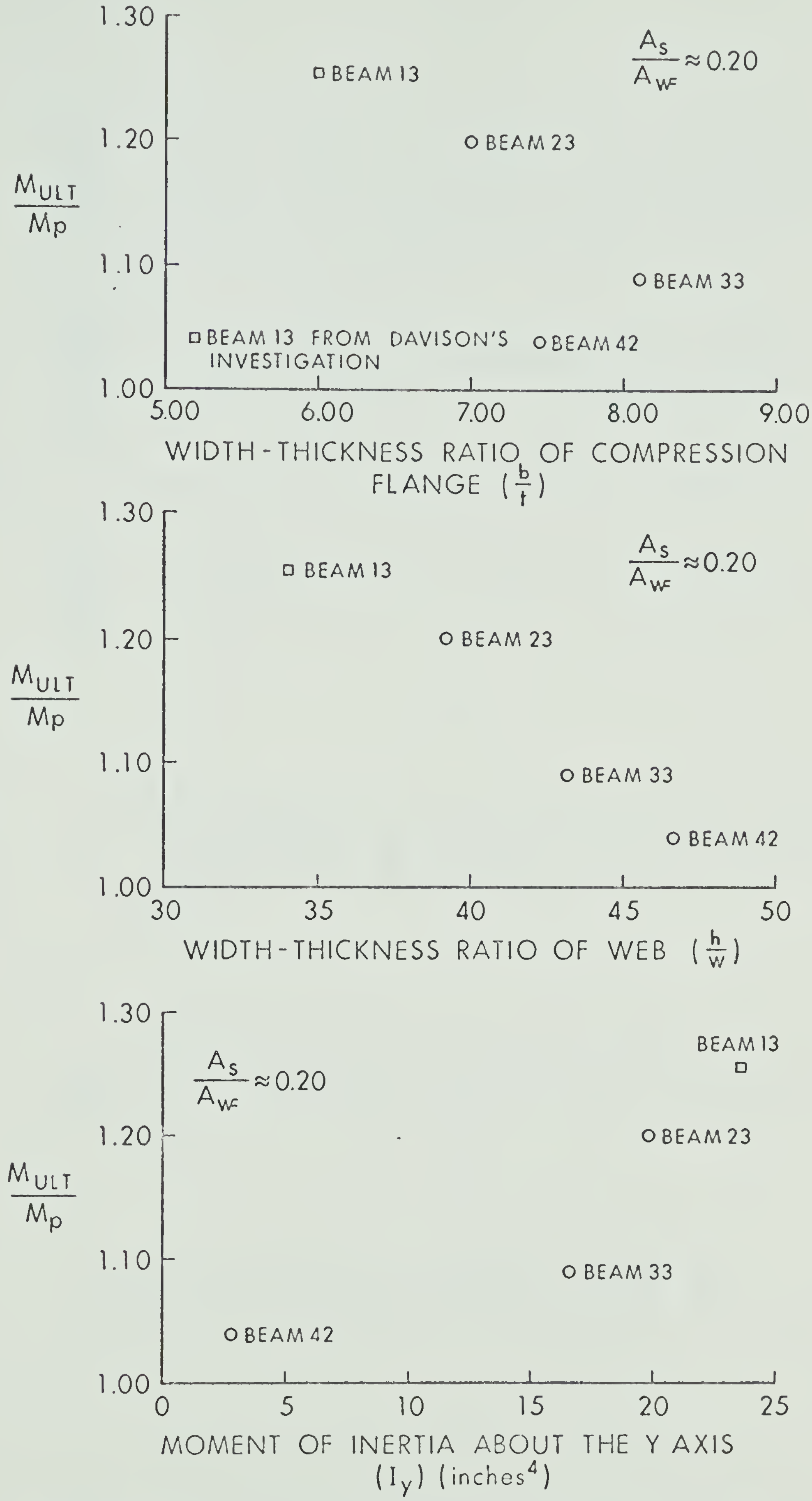

FIGURE 3·28 RELATIONSHIPS BETWEEN THE RATIO M_{ULT}/M_p AND STEEL SECTION PARAMETERS

TABLE 3.1

TEST RESULTS

BEAM	P_{ULT} (kips)	M_{ULT} (ft.kips)	M_P (ft. kips)	M_{ULT}/M_P	M_{ULT}/M^{o}_{ULT}	M_P/M^{o}_P
21	120	215.0	153.0	1.40	1.00	1.00
22	133	238.0	178.8	1.33	1.11	1.17
23	139	249.0	206.9	1.20	1.16	1.35
24	140	251.0	209.8	1.19	1.17	1.37
25	135	242.0	217.4	1.11	1.13	1.42
31	105.7	189.0	154.1	1.23	1.00	1.00
32	111.5	200.0	177.6	1.13	1.06	1.15
33	120.0	215.0	196.5	1.09	1.14	1.28
34	126.0	225.5	218.6	1.03	1.19	1.42
41	46	82.3	77.6	1.06	1.00	1.00
42	62	111.0	106.5	1.04	1.35	1.37
43	67	120.0	124.5	.96	1.46	1.55

TABLE 3.2

ROTATIONS AND CURVATURES AT ULTIMATE MOMENT

BEAM NUMBER	M_{ULT} (ft.kips)	$\emptyset_{ULT}$ rad/inx10^{-6}	θ_{ULT} radx10^{-3}
21	215.0	-	-
22	238.0	-	117
23	249.0	2550	69
24	251.0	-	69
25	242.0	800	54
31	189.0	13800	130
32	200.0	3000	66
33	215.0	-	40
34	225.5	1050	30
41	82.3	1500	57
42	111.0	1460	32
43	120.0	1460	29

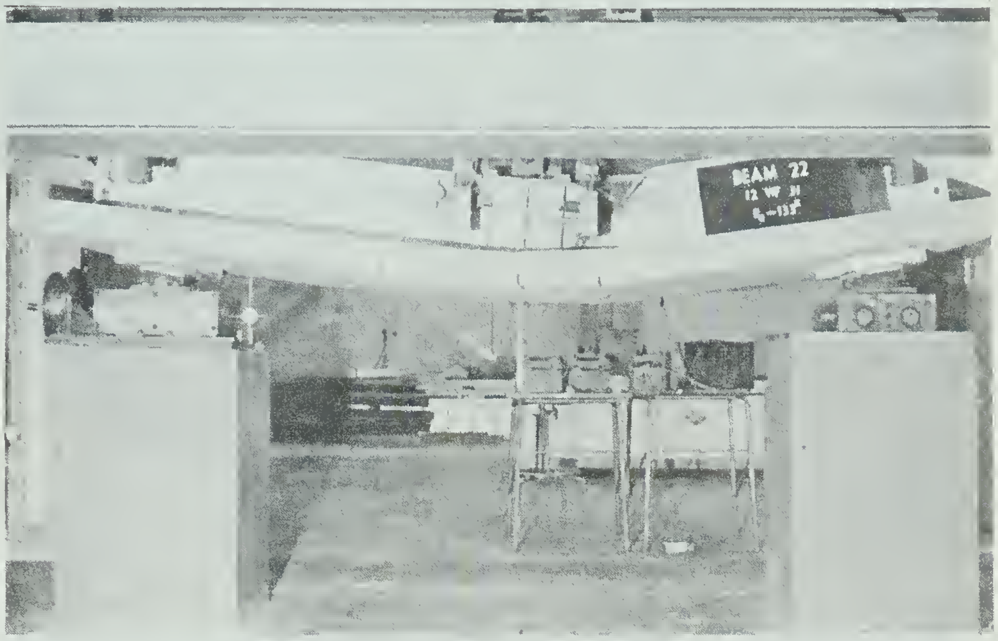

PLATE 3.1 TYPICAL APPEARANCE AT FAILURE

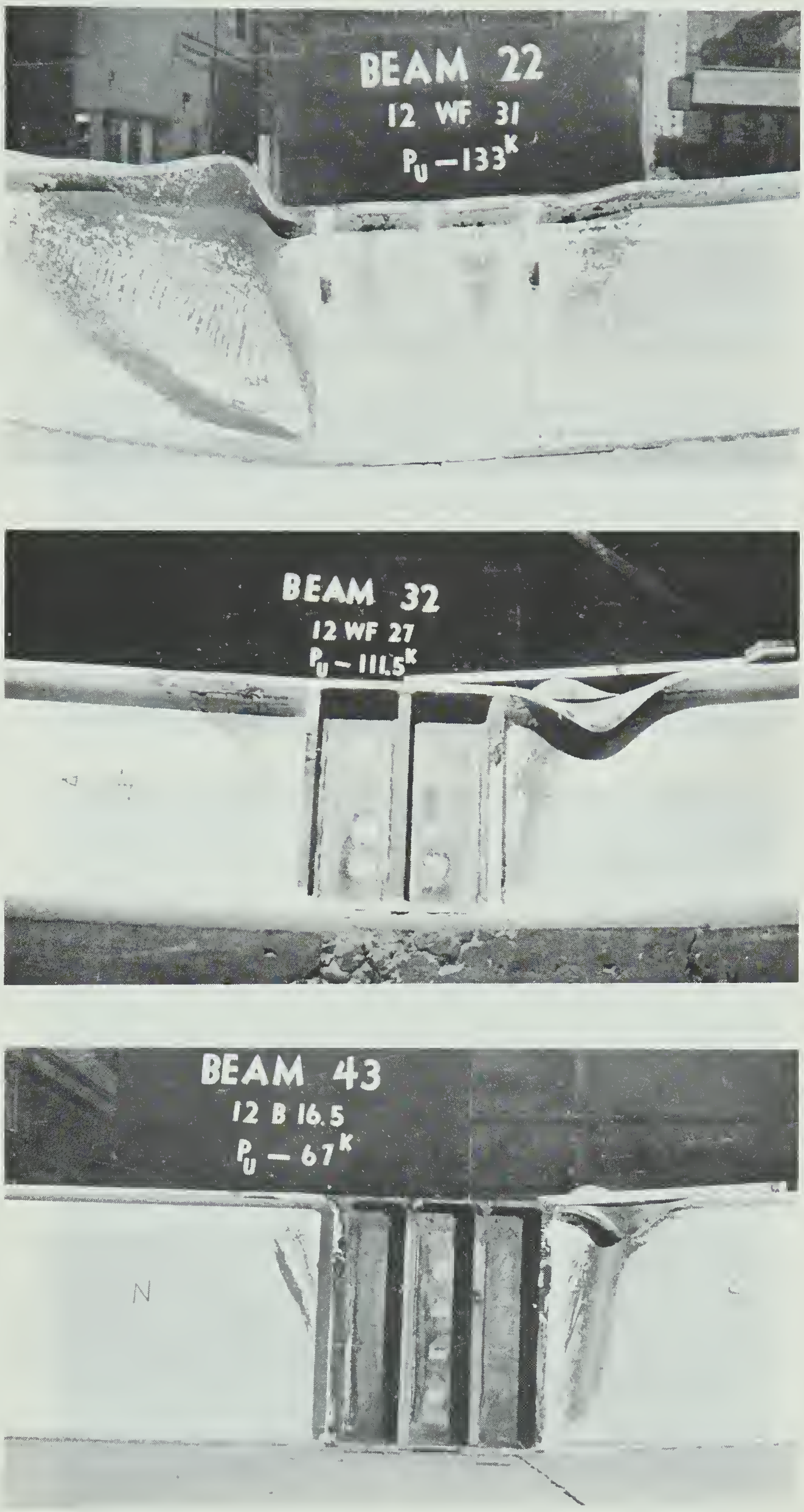

PLATE 3.2 TYPICAL LOCAL BUCKLES

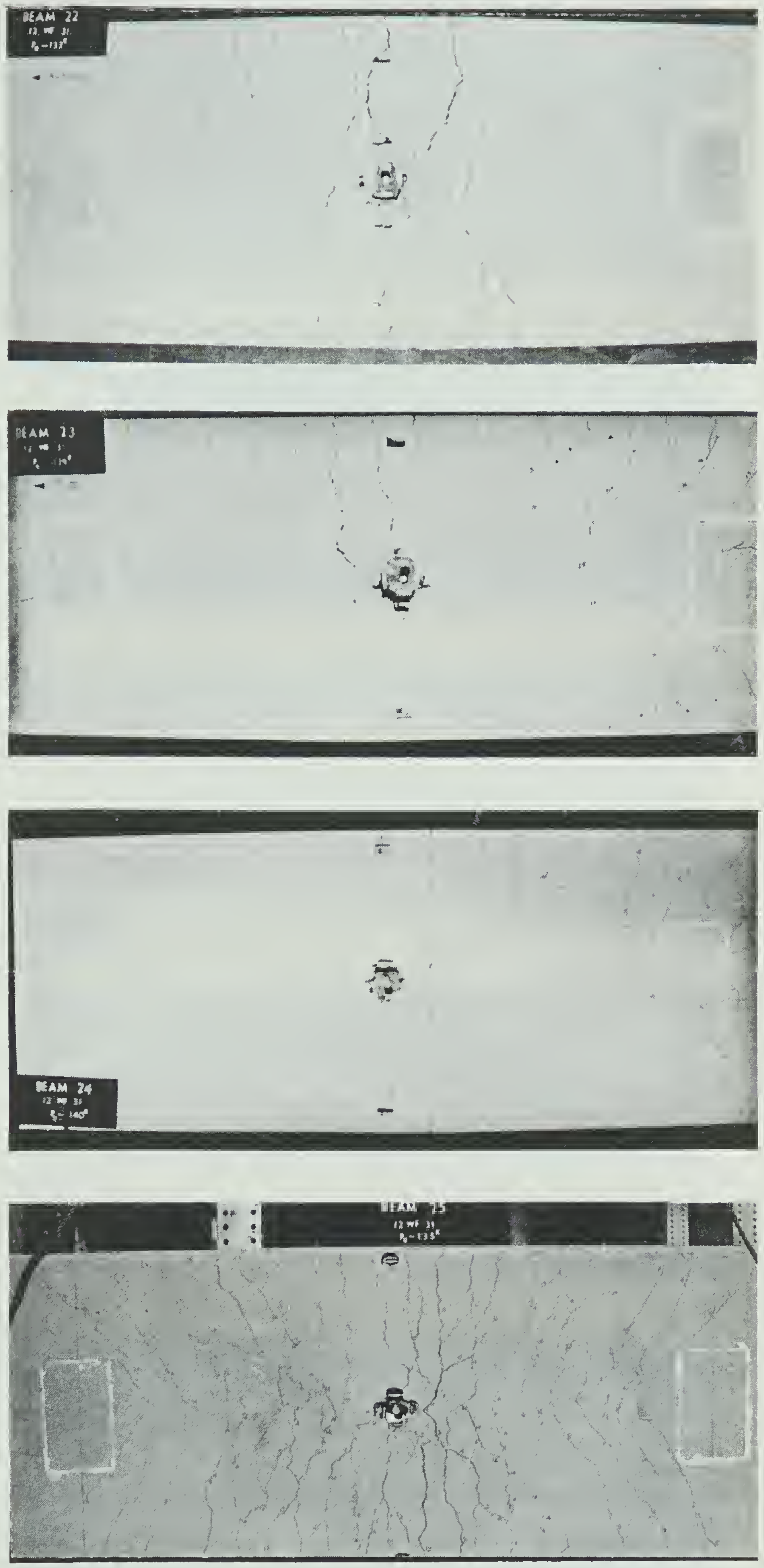

PLATE 3.3 CRACK PATTERNS

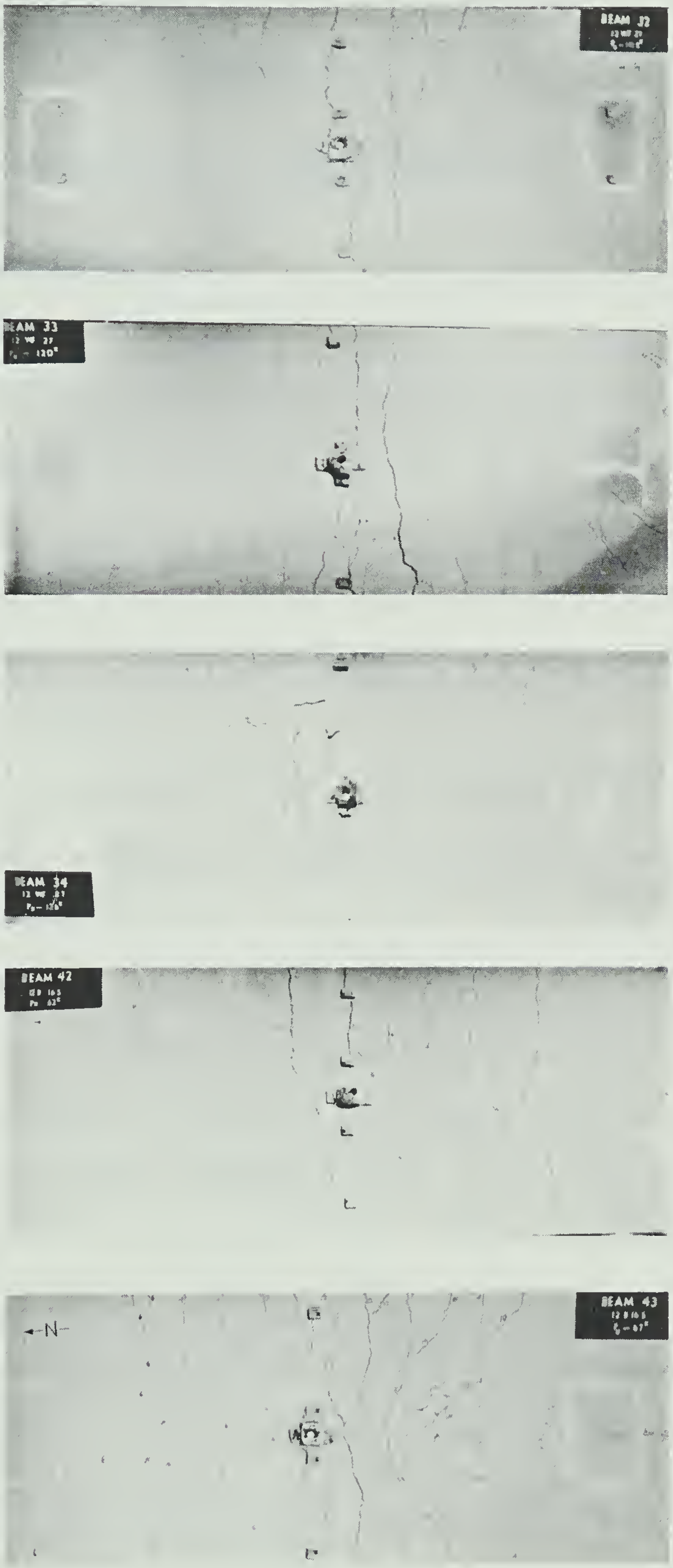

PLATE 3.4 CRACK PATTERNS

CHAPTER IV

DISCUSSION OF TEST RESULTS

4.1 GENERAL BEHAVIOR

Some difficulty was experienced in maintaining a vertical load during testing. This was due to initial warping in the rolled steel section which caused the beam to twist as the load was increased. Therefore, steel shims were placed under the loading bridge in an attempt to maintain a vertical load. The shimming process was repeated several times in each test.

The behavior of all beams under increasing load to ultimate was similar. However, once ultimate load was reached and local buckling occurred, the beams unloaded at different rates. The rate of unloading depended on the size of the steel section and the ratio of the longitudinal slab reinforcement to area of the steel section. At loads below the calculated simple plastic load, deflections were proportional to the applied load. Above the calculated simple plastic load, specimens deflected at an increasing rate. After local buckling, rotation was concentrated at the local buckle. All tests were terminated at maximum extension of the loading jack.

4.2 LOAD-DEFLECTION RELATIONSHIPS

The load-deflection relationships in FIGURES 3.1, 3.2, and 3.3 indicate that with increase in amount of longitudinal slab reinforcement, the ultimate load increased, but the deflection at ultimate decreased. As the longitudinal slab reinforcement increased unloading after ultimate load occurred more rapidly. The deflection behavior of the plain steel sections is also shown for comparison in the figures. FIGURE 3.4 shows that, for a given $\frac{As}{A_{WF}}$ ratio, the ultimate load increased as the size of the steel section was increased. The deflection at ultimate was also increased but the rate of unloading was decreased. FIGURE 3.5 indicates that for the plain steel beams, the deflection at ultimate load and the length of the plastic plateau increased with increase in steel beam size.

4.3 MOMENT-CURVATURE RELATIONSHIPS

The moment-curvature relationships shown in FIGURES 3.6, 3.7, and 3.8 indicate that with an increase in longitudinal slab reinforcement, the ultimate moment increased but the curvature decreased. However, BEAM 25 showed a reduction in both. This reduction resulted from using an amount of longitudinal reinforcement which placed the neutral axis well into the tension flange, thereby increasing the compressive stresses in the flange and forcing the web to local buckle prematurely. Generally at ultimate,

there was a rapid drop in moment with little change in curvature.

For the plain steel beams tested the curvature at ultimate moment increased with an increase in the size of the steel section as indicated in FIGURE 3.9. The wide flange beams exhibited a plastic plateau, the slope of which increased with an increase in the size of steel section. For the 12B16.5 section, there was little evidence of plastic deformation prior to failure by local buckling. Using a non-dimensional moment scale, the most heavily reinforced beams in each of the three series (BEAMS 25, 34, and 43) are compared in FIGURE 3.10. For similar $\frac{A_s}{A_{WF}}$ ratios, ultimate moment capacity increased and curvature decreased with increase in size of steel section.

Curvatures were derived from strain distributions across the steel section at midspan. As the load approached the simple plastic load, gages located on the face of the compression flange ceased to function and only those close to the neutral axis could be used in determining curvature. After buckling, most of the gages were unreliable and only a few curvatures could be plotted for the unloading portion of the moment curvature diagram. The longitudinal slab reinforcement affects the curvature at which buckling of the web and compression flange occurs. Moment-curvature relationships for BEAMS 22, 24, and 33 are not available since strain gages were omitted on these beams.

4.4 ROTATION CAPACITY

The total rotation of the beams obtained from summing the two end rotations is plotted against load in FIGURES 3.11, 3.12, and 3.13. The curves indicate that an increase in longitudinal slab reinforcement resulted in a decrease in rotation capacity. An increase in longitudinal slab reinforcement increases the depth of the steel section in compression, thereby increasing the tendency of the web to buckle and limiting the rotation capacity. Once buckling occurred there was a sudden drop in moment with little change in rotation after which the rate of rotation increased. FIGURE 3.14 indicates that for a given $\frac{As}{A_{WF}}$ ratio increasing the beam size resulted in an increased rotation at ultimate. FIGURES 3.15, 3.16, and 3.17 indicate that at a section located 5 in. from midspan on the end of the beam away from the local buckle, the rotation at ultimate moment was only slightly reduced with an increase in longitudinal slab reinforcement. After the attainment of ultimate moment there was a rapid reduction in moment, then the rotation rate increased due to concentration of the rotation about the local buckle. For BEAM 41 the lateral torsional mode of failure restricted rotation after ultimate. FIGURE 3.18 indicates that for a given $\frac{As}{A_{WF}}$ ratio the rotation of a section 5 in. from midspan at ultimate moment, increased with an increase in the size of the steel section.

4.5 LONGITUDINAL STRAINS AT MIDSPAN

Strains in the longitudinal slab reinforcement are plotted against applied load in FIGURES 3.19 and 3.20. Generally, at loads below the simple plastic load a linear relationship existed between applied load and longitudinal slab reinforcement strain. For a given steel section, an increase in the longitudinal slab reinforcement resulted in a reduced strain rate. With increasing load, strains increased more rapidly in the bars near the longitudinal centerline than in those near the slab edges. In BEAMS 22 and 32 the longitudinal reinforcement yielded at relatively low loads. For the remaining beams, the bars nearest the centerline yielded at loads approximately equal to the simple plastic load while those nearest the edge of the slab yielded at loads near the ultimate load. For the most heavily reinforced beams (BEAMS 25 and 34) the edge bars yielded after ultimate moment was reached.

4.6 TRANSVERSE REINFORCEMENT STRAINS

FIGURE 3.21 indicates the progression of strain in the transverse bars nearest midspan. Points plotted represent an average strain on two bars symmetrically positioned about the midspan. As the amount of longitudinal slab reinforcement increased the strain at ultimate decreased. At loads below the calculated simple plastic load, the transverse bars were subjected to small compressive strains. As ultimate load

was reached the transverse bars strained rapidly due to transverse bending of the slab. The transverse reinforcement in BEAMS 25 and 32 was in tension throughout the loading range. In BEAM 32 the transverse reinforcement yielded at a load approximately equal to 50 percent of the ultimate load. For the remaining beams, the transverse reinforcement yielded after buckling of the section occurred. Most strain gages ceased to function after the yield strain was reached.

4.7 LOAD-SLIP RELATIONSHIP

In composite beams, the degree of interaction is determined by the amount of slip between the concrete slab and the steel section. FIGURE 3.22 indicates that generally the slip at ultimate load increased with an increase in longitudinal slab reinforcement. For example, the slip measured at ultimate load was .0018 in. in BEAM 23, .0024 in. in BEAM 24, and .005 in. in BEAM 25.

For the first few increments of load no slip was recorded, but as the load increased and cracks developed, slip occurred and increased with load. Most of the slip occurred at loads above the calculated simple plastic load. The slip recorded for BEAMS 42 and 43 indicated that the steel section elongated more than the slab. This was due to inadequate shear transfer between the slender beam and stiff slab. Sudden cracking in some of the beams caused instantaneous slippage. After the local buckle formed in BEAM 32, the slip was reduced. Although the behavior of the

individual beams varied, the amount of slip at each end of the beam was similar prior to local buckling, then the slip was concentrated at the end closer to the buckle. The increased slip at the buckled end resulted from the fact that the shear connectors at that end resisted most of the longitudinal shear force after buckling.

4.8 CRACKING OF THE CONCRETE SLAB

PLATES 3.3 and 3.4 illustrate the cracking of the test specimens. Transverse flexural cracks developed at low loads near midspan perpendicular to the span. The location of these cracks coincided with the location of transverse bars in the slab. As the load increased, more transverse cracks developed along the span, and existing cracks widened. Diagonal cracking began at loads near the calculated simple plastic load. These diagonal tension cracks caused by shear transfer in the slab progressed from the centerline towards the edge of the slab across existing transverse cracks. Most cracks did not extend through the depth of the slab. At failure several transverse cracks near midspan expanded as a result of increased rotation resulting from the formation of the local buckle.

The crack pattern depended on the amount of longitudinal slab reinforcement, the spacing of the transverse slab reinforcement, and the transverse bending of the slab at high loads. Heavily reinforced slabs developed a large network

of diagonal tension and flexural cracks. Lightly reinforced slabs developed a few widely spaced transverse flexural cracks, interconnected by several diagonal tension cracks. As the number of cracks increased, the average crack width decreased.

4.9 ULTIMATE LOAD CONDITIONS

TABLE 3.1 compares observed ultimate moment capacity with theoretical simple plastic capacity. These values have been used in several plots to show the effect of longitudinal slab reinforcement and the size of steel section on the ultimate moment capacity. FIGURE 3.24 compares the ultimate behavior of all beams tested including those tested by Davison[1] and Piepgrass[2]. In all cases it was evident that an increase in amount of longitudinal slab reinforcement resulted in a reduction in the ratio of ultimate moment to theoretical plastic moment (M_{ULT}/M_P). However, the rate at which this ratio was reduced depended on the size of the steel section. For a given $\frac{As}{A_{WF}}$ ratio the M_{ULT}/M_P ratio increased with an increase in the size of the steel section. For the 12WF36 an almost linear relationship existed between the tension force in the longitudinal reinforcement and the ultimate moment capacity. With decreasing size of steel section and increasing amounts of longitudinal reinforcement ($\frac{As}{A_{WF}}$ below 0.2), web buckling was more prevalent due to the neutral axis moving closer to the tension flange. This

resulted in a noticeable reduction in the M_{ULT}/M_p ratio and an increase in the initial slope of the curves presented in FIGURE 3.24 Once the neutral axis reached the tension flange, the M_{ULT}/M_p ratio was not significantly influenced by a further increase in slab reinforcement. For the 12B16.5 series, the relationship between M_{ULT}/M_p and the total tensile force in the longitudinal reinforcement was significantly different from the relationships exhibited by the wide flange series. The difference in the relationship was attributed to the failure mode of the plain steel beam.

The increase in moment capacity with increase in slab reinforcement is shown in FIGURE 3.25 in the form of a plot of the ratio of ultimate moment of the composite beam to the ultimate moment of the plain steel section ($M_{ULT}/M^{O}{}_{ULT}$) against the total tensile force in the longitudinal reinforcement (A_sF_y) for all the beams in the present investigation and BEAMS 11, 12, 13 and 14 of Davison's investigation. For the 12B16.5 series it was evident that an increase in the amount of longitudinal reinforcement resulted in a substantial increase in the $M_{ULT}/M^{O}{}_{ULT}$ ratio. The wide flange sections, however, exhibited a gradual increase for low amounts of longitudinal reinforcement. Above the limit of reinforcement which placed the neutral axis into the tension flange, the increase was small. The behavior of the 12WF31 series tended to indicate that for ratios of $\frac{As}{A_{WF}}$ greater than 0.35, there was a reduction in the $M_{ULT}/M^{O}{}_{ULT}$ ratio. The actual increase in $M_{ULT}/M^{O}{}_{ULT}$ for

increasing amounts of slab reinforcement was not as great as that predicted by the theoretical M_p/M^o_p ratio for the wide flange sections. However, that for the 12B16.5 sections was almost the same. The difference between the calculated and experimental values increased with an increase in amount of longitudinal slab reinforcement. This indicated that the increase in ultimate moment was not directly proportional to the increase in theoretical plastic moment values. This trend was due to the different stability conditions of the web and the increased stiffness contributed by the slab to the tension flange. Plots showing the increase in the ratio, theoretical plastic moment of the composite beam to the theoretical plastic moment of the steel beam (M_p/M^o_p) with an increase in longitudinal reinforcement are presented in FIGURE 3.26

FIGURES 3.27 and 3.28 present the relationships between the ultimate moment capacity and the properties of the steel sections. Points plotted are for composite beams with a similar $\frac{As}{A_{WF}}$ ratio. In the present investigation, the width to thickness ratios of the web and compression flange $(\frac{b}{t}$ and $\frac{h}{w})$ were changed simultaneously. Since there is an interaction relationship between the two ratios, the plots must be considered as an oversimplification of the individual behavior of the web and flange. As these ratios decreased ultimate moment values increased. From the plots it would seem that the ultimate moment capacity was dependent primarily

on the width to thickness ratio of the web. An almost linear relationship exists between the M_{ULT}/M_p and the $\frac{h}{w}$ ratios. From the plot of M_{ULT} versus $\frac{b}{t}$, it is possible that the reason why the result for the 12B16.5 does not fall on the trend line is that the web buckling was the governing mode of failure. BEAM 13 from Davison's investigation is shown for comparison.

TABLE 3.2 presents the ultimate moment values and the corresponding rotation capacities. For beams with similar $\frac{As}{A_{WF}}$ ratios (BEAMS 23, 33 and 42), increasing the size of the steel section from a 12B16.5 to 12WF31 doubled the rotation at ultimate moment. This indicates that an increase in the size of the steel section definitely improves the rotation capacity of composite beams in negative bending. For the 12WF31 and 12WF27, increasing the $\frac{As}{A_{WF}}$ ratio from 0.1 to 0.2 resulted in a 5 and 8 percent increase in ultimate moment and a 41 and 21 percent reduction in rotation, respectively. Therefore, the 12WF31 section developed a smaller increase in moment than the 12WF27, but a higher reduction in rotation capacity. However, the net rotation of the 12WF31 was larger than that of the 12WF27.

4.10 LOCAL BUCKLING

All beams, except BEAMS 21 and 41, failed by local buckling of the web and compression flange near the load points. Prior to failure the load deflection relationships for the beams were almost linear. Yield lines developed in the web and compression flange near the load points

progressing towards the ends as load increased. The extent of yielding increased with a reduction in longitudinal reinforcement and an increase in the size of the steel section. Vertical shear yield lines developed near the supports at loads approximately equal to the simple plastic load. After sufficient yielding, BEAMS 22, 23 and 24 gradually formed a web and flange buckle while BEAM 25 buckled suddenly. The sudden failure of BEAM 25 was probably caused by the large stress in the extreme compression fibers due to the location of the neutral axis well into the tension flange. BEAMS 32, 33 and 34 failed rapidly by simultaneous buckling of the web and compression flange. Failure in BEAMS 42 and 43 was by web buckling. BEAM 21 was unloaded before failure and BEAM 41 exhibited a lateral torsional mode of failure due to the initial warped condition of the beam. All developed a slight lateral buckle at failure. PLATE 3.2 shows the typical yield pattern and local buckles. For composite beams in negative bending, the web is subjected to combined axial force and bending thereby increasing the depth of compression and the susceptibility to buckling. Attempts have been made to predict the local buckling behavior of beams subjected to combined axial load and bending. Haaijer and Thurlimann[11] recommended width to thickness ratio limits for the web of compact sections under combined axial load and bending. These ratios are based on theoretical and experimental results, and depend on the maximum strain, stress

distribution, and the yield stress of the material. A section meeting the suggested limits can be strained into the strain hardening region with no buckling occurring prior to the formation of a negative hinge. Bleich [12] also investigated the buckling behavior of plates under varying degrees of end restraint subjected to combined axial load plus bending. However, the results from his investigation are based on a material which does not strain harden, therefore, his results cannot be applied directly to steel sections. Lay and Galambos [13, 14] discussed the inelastic behavior of wide flange beams under a moment gradient. Lay examined the minimum width to thickness ratio of a compression flange which will allow the attainment of strain hardening before local buckling. When the beam is under a moment gradient local buckling of the flange can only occur when the yielded length equals the length of a potential local buckle. This length is dependent on the material, geometry of the section, and the value of moment at which the flange begins to yield. Due to the complexity of the buckling problem, width to thickness ratios were derived in the above studies for particular ratios of ultimate strain to yield strain, area of flange to area of web and for mild steels. Therefore, it is not possible to apply these methods directly to the beams in the present investigation.

CHAPTER V

SUMMARY CONCLUSIONS AND RECOMMENDATIONS

5.1 SUMMARY

The objectives of this investigation were to study the behavior of composite beams in an isolated negative moment region, with respect to the effects of varying the size of steel section and amount of longitudinal slab reinforcement. To achieve these objectives 12 tests were conducted on beams with varying amounts of reinforcement and 3 different steel sections. The beams were tested to failure by applying a statically incremented load. Failure of the beams was by local buckling of the web and compression flange.

5.2 CONCLUSIONS

The following conclusions are drawn from an analysis of the test results. These conclusions are supported by Davison(1) and Piepgrass(2) in previous investigations.

1. For a given steel section, significant increases in the ultimate moment capacity of composite beams in negative bending can be achieved by the addition of longitudinal slab reinforcement.

2. The increase in ultimate moment value (Mult) is not directly proportional to the increase in the theoretical plastic moment value (Mp).
3. For a given steel section, an increase in amount of longitudinal slab reinforcement results in a significant reduction in the rotation capacity of a negative plastic hinge. Therefore, to ensure the formation of a mechanism in continuous composite beams where the negative hinge is first to form, it may be necessary to limit the amount of longitudinal slab reinforcement.
4. Slip between the concrete slab and steel section increases with load. After a buckle forms, slip is concentrated in the region of the beam nearest to the buckle.
5. Slip between the concrete slab and the steel section significantly affects the strains in the longitudinal reinforcement. These strains are appreciably less than values determined from strain profiles in the steel section. However, at ultimate load strains reach the yield value.
6. The cracking behavior of the concrete slab is influenced by the amount of longitudinal slab reinforcement, the spacing of the transverse reinforcement, and the transverse curvature of

the slab. For low amounts of reinforcement a few wide cracks develop. As the amount of slab reinforcement increases, the number of cracks increases and the width of the cracks decreases.

5.3 RECOMMENDATIONS

It is evident that for the beams tested, the width to thickness ratios of the web and compression flange influence the rotational behavior of composite beams in negative bending. Therefore, it is recommended that for ultimate strength design of continuous composite beams, limits be placed on these ratios to ensure adequate rotation of the negative plastic hinge, so that the full moment capacity can be developed at the positive hinge locations. In this investigation the 12WF31 steel section exhibited the desired rotational behavior. Addition of longitudinal slab reinforcement also influences the rotation, therefore, an upper limit should be placed on the $\frac{As}{A_{WF}}$ ratio. This limit should be no greater than that related to the amount of longitudinal slab reinforcement required to bring the neutral axis to the tension flange.

If the theoretical plastic moment (M_P) is used as an indicator for the ultimate moment (M_{ULT}), it must be realised that the ratio $\frac{M_{ULT}}{Mp}$ is not a constant but decreases as the theoretical plastic moment (M_P) increases.

BIBLIOGRAPHY

1. Davison, J.H., "Composite Beams in Negative Bending", Masters Thesis, Department of Civil Engineering, University of Alberta, May 1969.

2. Piepgrass, E.B., "Behavior of Composite Beams in Negative Bending", Masters Thesis, Department of Civil Engineering, University of Alberta, June 1968.

3. Ferrier, D., "Moment Curvature Relationship of Composite Steel and Concrete Beams", Masters Thesis, Department of Civil Engineering, University of Alberta, November 1965.

4. Barnard, Peter R., "On the Collapse of Composite Beams", a disertation submitted to the University of Cambridge for the degree of Doctor of Philosophy, Corpus Christi College, September 1963.

5. Johnson, R.P., "Research on Composite Steel - Concrete Beams, 1960 - 1968", Meeting Preprint, American Society of Civil Engineers, April 1969.

6. Barnard, P.R., and Johnson R.P., "Ultimate Strength of Composite Beams", Proc. Inst. Civ. Eng., Vol. 32, October 1965, pp. 161 - 179.

7. Barnard, P.R., and Johnson, R. P., "Plastic Behavior of Continuous Composite Beams", Proc. Inst. Civ. Eng., Vol. 32, October 1965, pp. 180 - 197.

8. Johnson, R.P., Finlinson, J.C.H., and Heyman, J., "A Plastic Composite Design", Proc. Inst. Civ. Eng., Vol. 32, Oct. 1965, pp. 198 - 209.

9. van Dalen, K., "Composite Action at the Supports of Continuous Beams", Ph.D. Thesis, University of Cambridge, 1967.

10. Johnson, R.P., van Dalen, K., and Kemp, A.R., "Ultimate Strength of Continuous Composite Beams", Proceedings, Conference of Structural Steelwork, London, Sept. 1966, pp. 27 - 35, British Constructional Steelwork Association.

11. Haaijer, G., and Thurlimann, B., "Inelastic Buckling in Steel" Paper No. 3023, Transactions, ASCE, Vol. 125, 1960.

12. Bleich, F., "Buckling Strength of Metal Structures", McGraw - Hill Book Co., New York, N.Y. 1952.

13. Lay, M.G., "Flange Local Buckling in Wide-Flange Shapes", Journal of the Structural Division, Proc. ASCE, Vol. 91, No. ST6, December 1965, p. 95.

14. Lay, M.G., and Galambos, T.V., "Inelastic Beams Under Moment Gradient", Journal of the Structural Division, Proc. ASCE, Vol. 93, No. ST1, February 1967, p. 381